

Stochastic Atmospheric Forcing as a Cause of Greenland Climate Transitions

HANNAH KLEPPIN AND MARKUS JOCHUM

Niels Bohr Institute, University of Copenhagen, Copenhagen, Denmark

BETTE OTTO-BLIESNER, CHRISTINE A. SHIELDS, AND STEPHEN YEAGER

National Center for Atmospheric Research, Boulder, Colorado

(Manuscript received 24 October 2014, in final form 19 June 2015)

ABSTRACT

An unforced simulation of the Community Climate System Model, version 4 (CCSM4), is found to have Greenland warming and cooling events that resemble Dansgaard–Oeschger cycles in pattern and magnitude. With the caveat that only three transitions were available to be analyzed, it is found that the transitions are triggered by stochastic atmospheric forcing. The atmospheric anomalies change the strength of the subpolar gyre, leading to a change in Labrador Sea sea ice concentration and meridional heat transport. The changed climate state is maintained over centuries through the feedback between sea ice and sea level pressure in the North Atlantic. Indications that the initial atmospheric pressure anomalies are preceded by precipitation anomalies in the western Pacific warm pool are discussed. The full evolution of the anomalous climate state depends crucially on the climatic background state.

1. Introduction

Abrupt climate transitions occurring in the North Atlantic (NA) region and in particular at Greenland during the last glacial period, spanning the period from about 120 000 to 12 000 years ago, are well documented in various climate proxy archives, the most frequent ones being Dansgaard–Oeschger (D-O) events (Dansgaard et al. 1993). D-O events feature a distinct pattern of abrupt warming of 8°–16°C (e.g., Landais et al. 2004; Huber et al. 2006) followed by gradual cooling of the same amplitude, completing a so-called D-O cycle. The cold and warm phases are called Greenland stadials and interstadials, respectively. D-O cycles occur most frequently in Marine Isotope Stage 3 (MIS3) and are also associated with a reorganization in atmospheric circulation as inferred from various dust and deuterium excess measurements of Greenland ice cores (e.g., Steffensen et al. 2008). Consistent with the warming during Greenland interstadials, snow accumulation rate is 50%–100% increased relative to stadials (Andersen et al. 2006). D-O cycles coincide

with changes in the tropics and large parts of the Northern Hemisphere [an overview of paleoclimatic proxies indicating coinciding shifts with Greenland temperature can be found, e.g., in Rahmstorf (2002)]. Antarctic temperature changes are gradual and in antiphase with Greenland temperature over a D-O cycle (Barbante et al. 2006).

Interestingly there is also evidence for abrupt warmings at Greenland in the present day, although they are smaller in amplitude: around 1920 a warming of about 4°C at several meteorological stations at Greenland is reported by Cappelen (2013). The warming lasted over a decade and was followed by a slight cooling until the mid-1980s. Furthermore, Bond et al. (1997) suggest “mini-D-O events” during the Holocene based on ice rafted debris (IRD) changes in two marine sediment cores from the NA. These align with geochemical composition changes in the Greenland Ice Sheet Project 2 ice core, indicating atmospheric circulation changes over Greenland (O’Brien et al. 1995).

First hypotheses trying to explain D-O cycles were based on an abrupt shutdown of the Atlantic meridional overturning circulation (AMOC), initiated by freshwater input into the NA (e.g., Broecker et al. 1990), although the cooling phase of D-O cycles is not necessarily abrupt. More recent model studies revealed that the

Corresponding author address: Hannah Kleppin, Niels Bohr Institute, University of Copenhagen, Juliane Maries Vej 30, 2100 Copenhagen, Denmark.
E-mail: kleppin@nbi.ku.dk

amount of freshwater necessary to slow down the AMOC sufficiently to produce temperature changes at Greenland comparable to D-O cycles depends on model details (Kageyama et al. 2013; Manabe and Stouffer 1999; Dijkstra 2007), as well as on the location of the freshwater forcing (Mignot et al. 2007) and its timing (Bethke et al. 2012). Bethke et al. (2012) demonstrate that different models produce a wide range of outcomes for the deglaciation, given the same forcing. Furthermore, the evidence for freshwater input into the NA during D-O cycles is still subject to discussion. Based on sea level reconstructions from the Red Sea, Arz et al. (2007) suggest up to 25 ± 12 m global sea level rise at the onset of Greenland interstadials. On the other hand Siddall et al. (2003) and Rohling et al. (2008) suggest an increase of sea level of 30 ± 12 m during Greenland stadials.

Other mechanisms invoked to play a role in centennial to millennial scale AMOC variability and possibly in the dynamics behind D-O cycles are salt oscillators of the NA, not induced by meltwater pulses. Jackson and Vellinga (2013) find a salt oscillator due to interaction of tropical salinity anomalies [induced by a southward (northward) intertropical convergence zone (ITCZ) shift associated with AMOC weakening (strengthening)], and subpolar salinity anomalies due to decadal fluctuations of freshwater export through the Fram Strait. Peltier and Vettoretti (2014) find, by decreasing diapycnal diffusivity in a model simulation, that a salt oscillator of the glacial NA causes D-O-like temperature changes and AMOC variability. However, this contrasts with recent findings that suggest vertical diffusivities increased by a factor of 3 during Last Glacial Maximum (LGM) compared to preindustrial climate (Schmittner et al. 2015). Furthermore, evidence for AMOC shutdown during D-O cycles is ambiguous. A recent study finds instead that a strong AMOC prevailed during most parts of the last glacial period and shutdown of the AMOC occurred only during Heinrich events close to the LGM (Böhm et al. 2015).

Some of the more recent hypotheses trying to explain D-O events invoke sea ice–atmosphere interactions. Li et al. (2005) find that a reduction of sea ice extent can cause a climatic response consistent with D-O event signals of temperature and accumulation measured from Greenland ice cores. The authors point out that, in addition to the well-known ice–albedo feedback, sea ice strongly influences regional air temperatures by insulating the atmosphere from the ocean heat reservoir. The possibility of “switching the ocean–atmosphere heat exchange off” due to extensive sea ice cover provides a plausible mechanism for abrupt and large local temperature changes, even though the initial

forcing might be relatively small. Far-field signals and ocean–atmosphere feedbacks are not represented in their study, due to prescribed sea surface temperatures (SSTs) and an inactive ocean component. In their study the mechanism causing the displacement of the sea ice edge remains unexplored. Li et al. (2010) extend the previous study by implementing more realistic sea ice retreat scenarios. They find that the displacement of the sea ice edge in the Nordic seas causes a 10°C warming and 50% increase in accumulation at Greenland summit, whereas sea ice changes in the western NA have less effect.

Rasmussen and Thomsen (2004) find a subsurface warming during Greenland stadials based on the analysis of eight marine sediment cores taken from the Nordic seas and the NA. A new high-resolution sediment core from the Nordic seas confirms this subsurface warming (Dokken et al. 2013). They suggest a sequence of events that could explain a sudden melt of sea ice. In combination with the results of Li et al. (2005) this provides a possible mechanism for D-O events. During the stadial phase warm Atlantic inflow is separated from surface and sea ice by a strong halocline, allowing for an extensive ice cover to persist. The mechanism proposed to initiate the abrupt melting involves a slow subsurface warming during stadials due to the separation of the warm Atlantic inflow from the surface. Eventually this subsurface warming destabilizes the water column, the halocline collapses, and warm subsurface water can reach the surface and melt the sea ice (e.g., Dokken et al. 2013; Kim et al. 2012). Other hypotheses invoke ice sheet height variations as a trigger of D-O events. For instance Zhang et al. (2014) demonstrates that by varying the height of the Laurentide ice sheet a positive ocean–atmosphere–sea ice feedback is initiated eventually leading to D-O-like climate shifts.

Studying the climate response to highly idealized scenarios of prescribed external forcing (e.g., freshwater-hosing experiments, prescribing sea ice cover, or ice sheet changes) gives insight into the particular process and helps to determine its potential influence on Greenland temperatures. However, the origin of the prescribed external forcing remains unclear. To our knowledge there are only five examples of abrupt climate changes arising spontaneously in coupled climate models (i.e., without having been triggered by variations in external forcing). Hall and Stouffer (2001) describe a cooling event around Greenland in a fully coupled climate model with coarse resolution. The event lasts for a period of only 30–40 years and is caused by a persistent northwesterly wind anomaly transporting cold and freshwater into the NA and causing a shutdown of deep water convection. Goosse et al. (2002) describe

cooling events occurring in Earth System Models of Intermediate Complexity (EMIC). The cold events are attributed to a displacement of the oceanic deep water convection sites to a more southern location. Just as in [Hall and Stouffer \(2001\)](#) the shutdown of deep water convection is induced by stochastic atmospheric forcing, but in addition [Goosse et al. \(2002\)](#) demonstrate that such an event could also be triggered by appropriate changes in solar irradiance. The remaining three examples of spontaneous climate transitions occur in state-of-the-art fully coupled climate models. [Sidorenko et al. \(2015\)](#) report several events of sudden decrease of deep water convection and increase of Labrador Sea (LS) ice extent. The mechanism behind them is not studied in detail, but the authors attribute them to anomalously saline and warm water inflow into the deep LS. The anomalous light deep water weakens the subpolar gyre (SPG) circulation causing a change in the upper-LS freshwater budget. The warm and saline bias in the deep NA is mainly attributed to overly strong surface winds in the subtropical NA, modifying the path of Gibraltar Strait outflow in the NA. [Martin et al. \(2015\)](#) report on centennial-scale variability of the AMOC and other changes in the NA (e.g., SPG strength and NA heat content) driven by Southern Ocean deep water convection variability. The signal transmission to the NA occurs through an enhanced meridional density gradient between deep (below 1200 m) NA and South Atlantic and a compensation of Antarctic Bottom Water by increased NA deep water extent. [Drijfhout et al. \(2013\)](#) describe a spontaneous cold event with a duration of about 100 years. The authors attribute the cold event to a period of anomalous high atmospheric blocking above the eastern subpolar gyre. The blocking causes the sea ice edge to progress farther south in the Greenland Sea and eventually excites a cold core high pressure anomaly at the southwestern tip of Greenland. The anomalous anticyclone advects cold air through enhanced northerly winds to the sea ice edge, causing the sea ice extent to grow even farther. Additional sea ice is transported southward by ocean currents and causes a fresh surface anomaly in the LS. As a consequence deep water convection shuts off and due to longer exposure of the ocean surface to the atmosphere sea ice growth commences, reinforcing the atmospheric anomaly. The anticyclonic anomaly, now centered above the LS, causes a change from northerly to more southerly winds, advecting warm air, melting the sea ice, and returning the system to normal.

Here, we document three climate transitions occurring in a 1000-yr preindustrial control simulation of the Community Climate System Model, version 4 (CCSM4). These are two gradual cooling and one abrupt warming

event around Greenland. The analysis is focused on the first cooling event. The atmospheric anomaly during the cold event resembles closely the one described by [Drijfhout et al. \(2013\)](#). However, the evolution and hence the cause of the cold NA phase is different. It involves a strong positive feedback loop of the SPG circulation. The first weakening of the SPG is caused by decrease in wind stress curl associated with a stochastic atmospheric circulation anomaly. The decreased gyre circulation changes the salinity transport into the highly sensitive deep water convection site in the LS, thus reducing deep water convection and eventually affecting the AMOC. This is followed by an increase of sea ice cover and a drop in Greenland temperature. The increased sea ice cover itself forces a reorganization of the atmosphere, thus sustaining the anomalous atmospheric forcing of the gyre circulation for about 200 years.

The objective of this paper is to identify processes and regions of atmospheric, oceanic, and sea ice interactions that play a key role in the transitions between cold and warm NA phases and to suggest a consistent sequence of events causing these transitions. In [section 2](#) we give a brief overview of CCSM4, the setup of the control simulation, and the different experiments that we carried out. [Section 3](#) comprises the results structured as follows. We describe how the first cold event manifest itself in Greenland, the NA, and globally ([section 3a](#)), followed by a description of the stochastic atmospheric trigger [[section 3b\(1\)](#)], the dynamics of the ocean response and sea ice changes [[section 3b\(2\)](#)], and the atmospheric feedback [[section 3b\(3\)](#)]. The sequence of events leading to the abrupt warming is documented in [section 3c](#). Finally we assess the dependence of the proposed mechanism on the particular background climate ([section 3d](#)) and test the atmospheric trigger in forced ocean simulations ([section 3e](#)). In [section 4](#) we discuss our main findings and a possible influence of tropical temperature and precipitation anomalies on NA atmosphere circulation changes. The paper concludes with a summary in [section 5](#).

2. Model

The numerical experiments are performed using CCSM4, which consists of the fully coupled atmosphere, ocean, land, and sea ice models. A detailed description of this version can be found in [Gent et al. \(2011\)](#). The ocean component is POP, version 2 (POP2), and has a horizontal resolution that is constant at 1.125° in longitude and varies in latitude from 0.27° at the equator to approximately 0.7° at high latitudes. In the vertical there are 60 depth levels; the uppermost layer has a thickness of 10 m and the deepest layer has a thickness of 250 m.

TABLE 1. Simulations analyzed and conducted for this study. The letters G and B in column compset refer to ocean–sea ice simulations and the fully coupled version of CCSM, respectively. The setup of the different simulations is described in section 2.

Expt	Compset	Atmosphere		Length (yr)	Starting year	Starting from
		Resolution	Forcing			
CONT	B	2°	—	1000	—	—
HI	B	1°	—	1300	—	—
DO_F	G	2°	—	36	305	CONT
OI_a	G	—	DO_F year 332/333	11	311	HI
OI_b	G	—	DO_F year 312/313	30	299	HI
OI_c	G	—	DO_F year 312/313	21	311	HI
OI_d	G	—	DO_F year 312/313	13	321	HI
OI_e	G	—	DO_F year 305/306	13	299	HI
OI_f	G	—	DO_F year 305/306	13	327	OI_b
DO_a	G	2°	—	102	299	CONT
DO_b	G	2°	—	90	321	CONT
DO_c	G	2°	—	73	561	CONT
DO_d	G	2°	—	51	581	CONT
DO_e	G	2°	—	51	401	CONT
DO_f	G	2°	—	51	899	CONT
DO_X	G	2°	—	198	1001	CONT

The atmospheric component uses a horizontal resolution of $1.9^\circ \times 2.25^\circ$ (longitude by latitude) with 26 levels in the vertical. The sea ice model shares the same horizontal grid as the ocean model and the land model is on the same horizontal grid as the atmospheric model. This setup constitutes the released version of CCSM4, and

further details can be found in Danabasoglu et al. (2012). The subsequent sections will analyze and compare several different simulations listed in Table 1. The simulations are either conducted with the fully coupled version or the ocean–sea ice version with prescribed atmospheric fluxes and river run off. The main focus is

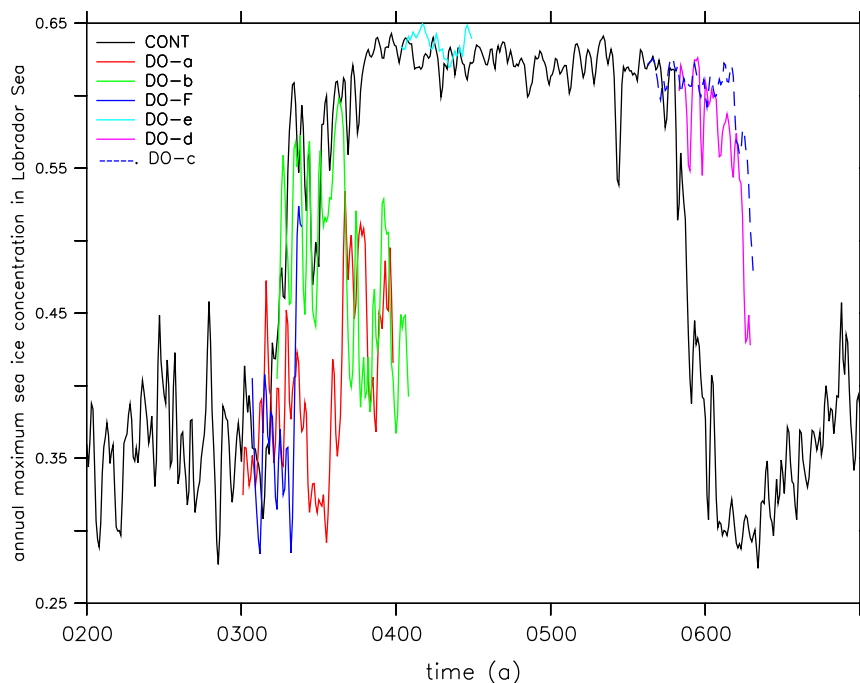


FIG. 1. Annual maximum sea ice concentration in the LS (averaged over 45° – 65° W and 50° – 70° W) for CONT (black). Additionally shown are the sea ice concentrations for the different branch runs (different colors). All curves are smoothed by a 2-yr running mean.

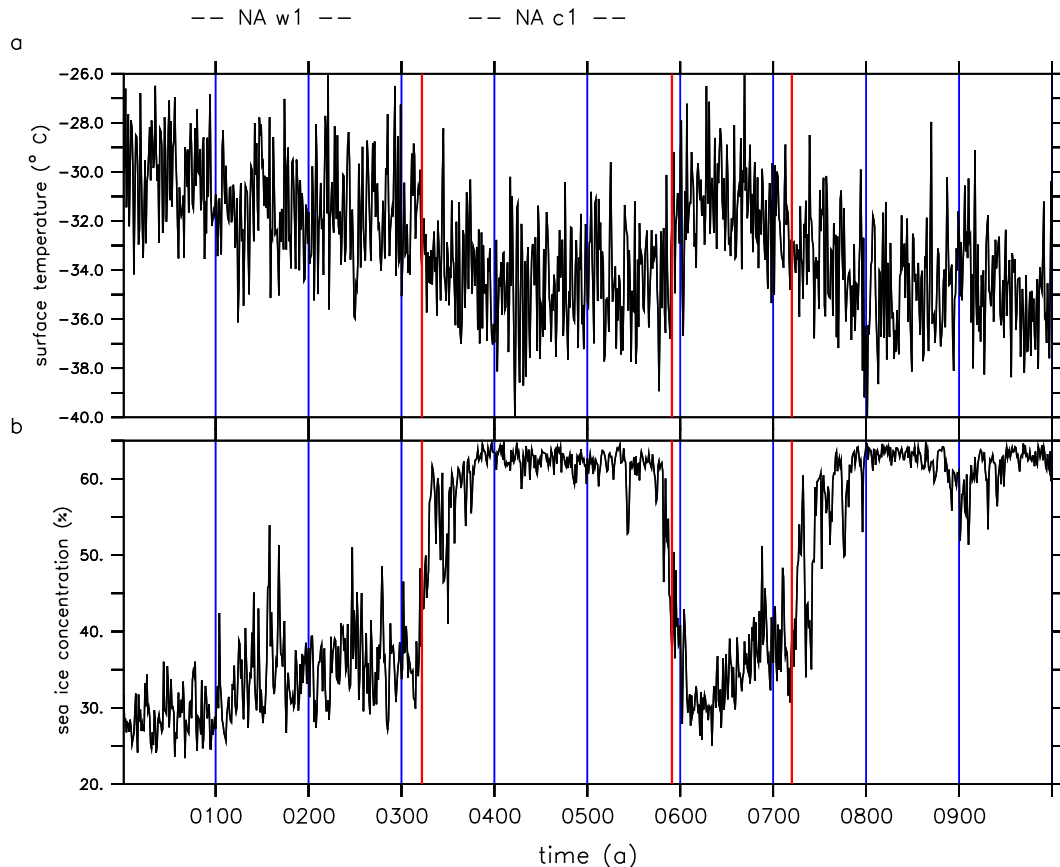


FIG. 2. (a) Greenland annual minimum surface temperature ($^{\circ}\text{C}$) averaged over $65^{\circ}\text{--}80^{\circ}\text{N}$, $55^{\circ}\text{--}15^{\circ}\text{W}$. (b) Annual maximum of sea ice concentration in the LS (as in Fig. 1). The different phases of interest are indicated on top, NA_w1 is the period from year 50 to year 250 and NA_c1 from year 350 to year 550. The transitions between different warm and cold phases, based on Greenland temperature changes, are marked by red horizontal lines.

on a 1000-yr-long preindustrial control simulation (CONT), in which Earth's orbital parameters are set to 1990 values and the atmospheric composition is fixed at its 1850 values [for details of the atmospheric composition, see Gent et al. (2011)]. For comparison with CONT and as initial conditions for some of the experiments described below we make use of another preindustrial control simulation (HI). HI differs from CONT only in the horizontal resolution of the atmospheric component which is $0.98^{\circ} \times 1.258^{\circ}$. An overview of differences and similarities between CONT and HI is provided by Shields et al. (2012) and discussed in section 3d.

Danabasoglu et al. (2012) and Danabasoglu et al. (2014) assess the fidelity of the CCSM ocean module. For CONT in particular we find that the AMOC is well represented at 26.5°N with a maximum of 18.4 Sv ($1 \text{ Sv} \equiv 10^6 \text{ m}^3 \text{ s}^{-1}$) at 1000 m, compared to the observed maximum of 18.6 Sv, also at 1000 m (Cunningham et al. 2007). The SPG circulation strength (spatial maximum of about 50 Sv) in CONT agrees fairly well with observations

by Johns et al. (1995) and Pickart et al. (2002) of 48 and 40 Sv, respectively.

In a 200-yr average over a period prior to the transitions CONT features a cold ($\sim 2^{\circ}\text{C}$) and fresh (0.2 psu) bias in the upper 100 m of the western SPG and the LS compared to temperature (Locarnini et al. 2010) and salinity (Antonov et al. 2010) data from the *World Ocean Atlas 2009* (WOA09). Below the surface the model is too warm and salty by about 1°C and about 0.3 psu, respectively. In both WOA09 and CONT, maximum mixed layer depths occur during March in the LS with values in excess of 1400 m.

To ensure that the transitions are not caused by any numerical or computational issues several runs branching from CONT were performed to test the reproducibility of the occurring transitions. The branch runs (DO_a through DO_f in Table 1) were started using initial conditions from CONT at different points in time. The initial conditions are modified by a random $O(\varepsilon)$ perturbation.

The branch runs reproduce the climate transitions [two warming (DO_c and DO_d) and three cooling

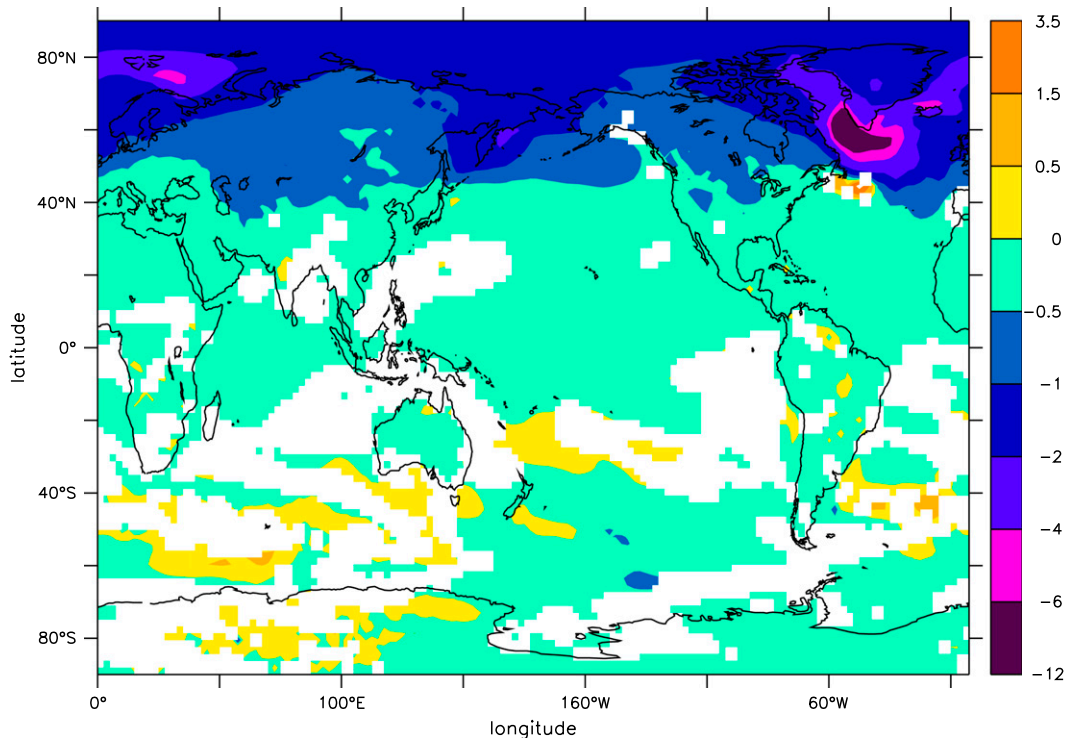


FIG. 3. Global temperature signal: surface temperature difference ($^{\circ}\text{C}$) between years 350–550 (NA_c1) and years 50–250 (NA_w1). Regions are only shaded if correlation with Greenland surface temperature (averaged over the same region as in Fig. 2) for the period between years 270 and 470 is significant on a 95% level.

(DO_a, DO_b, and DO_F) transitions] even though the transitions in the branch runs occur at different points in time and not always with the same amplitude as in CONT. The annual maximum sea ice concentration in the LS of the original CONT run (black) and the branch runs (different colors) are depicted in Fig. 1. The reproducibility of the climate transitions gives us trust in our findings beyond the lack of statistical analysis possibility. A 200-yr extension (DO_X) of CONT was conducted without any further transitions occurring; thus, the second cold phase lasts at least 400 years. Possible reasons for the lack of transitions in DO_X are discussed in section 4. This and the occurrence of the branch run transitions at different times suggest that a stochastic process triggers a switch between two climate states. Furthermore the different durations of the cold phases points to the fact that no particular buildup time for any kind of reservoir (e.g., warm subsurface water) is involved.

To test the proposed role of the stochastic atmospheric trigger, we conducted several ocean–ice (OI) simulations with different atmospheric forcings (Table 1). For this purpose a part of CONT was rerun, saving the atmospheric fluxes at 3-h intervals (DO_F run). The OI experiments were started from HI initial conditions

and were forced with annually repeating atmospheric fluxes from DO_F (July–June). The different starting years and the forcing year from DO_F are listed in Table 1. We chose starting years preceding a rapid sea ice increase in DO_F for experiments with transitions from a warm to a cold NA phase (OI_a through OI_d). Year 305/306 in DO_F precedes a rapid sea ice decrease and is utilized to reproduce the warming transition (OI_e and OI_f).

3. Results

a. Sequence of events

The preindustrial control simulation analyzed here features abrupt surface temperature changes in Greenland and in the whole Northern Hemisphere. In the entire simulation three transitions between warm and cold NA phases occur (Fig. 2a). Hereafter we refer to the first warm NA phase (years 50–250, as indicated in Fig. 2) as NA_w1 and to the first cold NA phase (years 350–550) as NA_c1. Over the first transition (first red line in Fig. 2) the annual mean Greenland temperature decreases gradually by approximately 3°C [averaged over Greenland (65° – 80°N , 55° – 15°W)]. This is followed by an abrupt warming of about the same

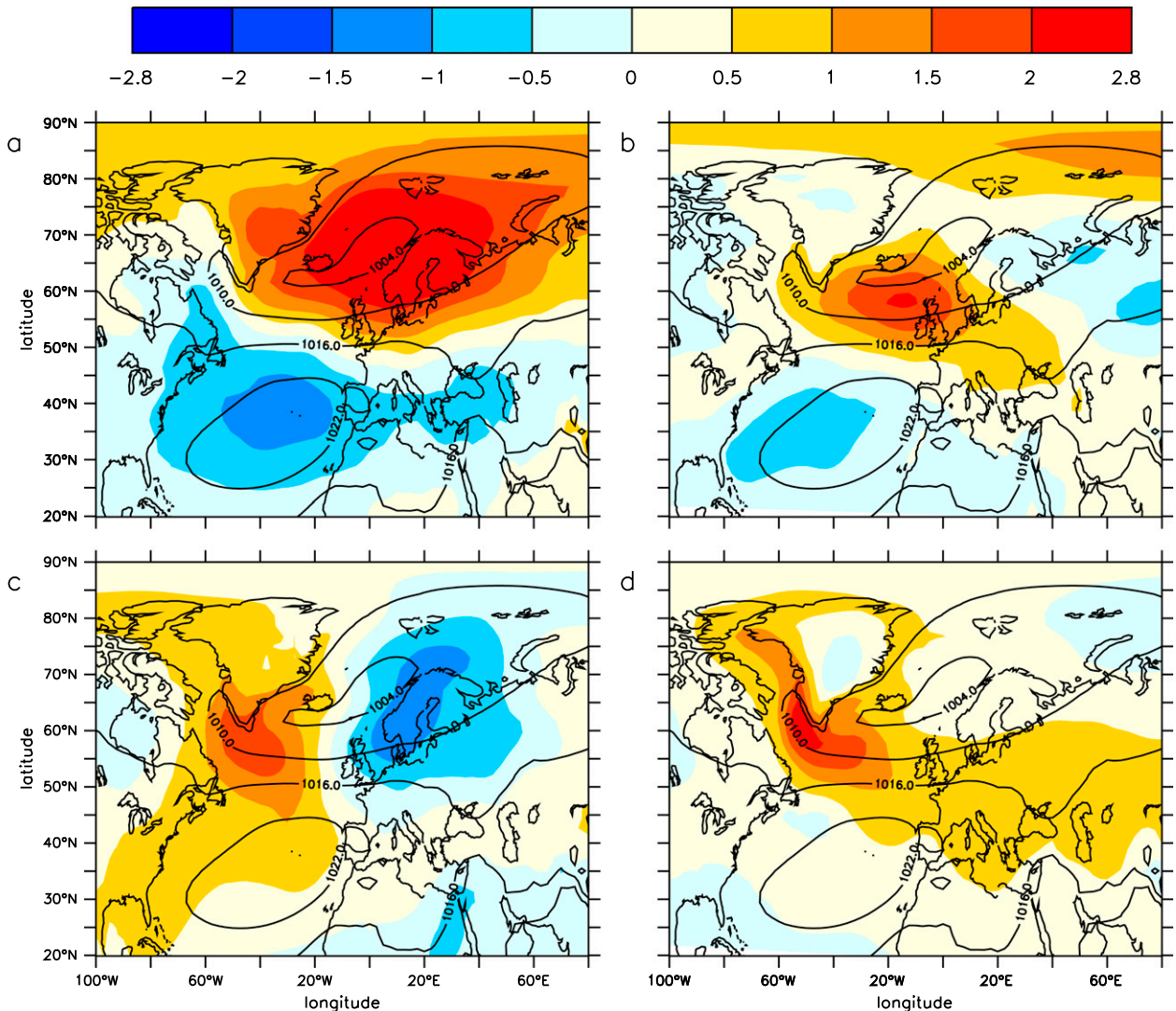


FIG. 4. Sea level pressure anomaly (hPa) for (a) years 310–315, (b) years 315–320, (c) years 320–325, and (d) NA_c1 (years 350–550). All anomalies are relative to NA_w1 and positive values imply a higher SLP than during NA_w1. Contours show the 1000-yr mean of SLP.

amplitude over the second transition (second red line in Fig. 2). At the southwestern coast of Greenland temperature changes are more than 3 times that value. Cooling and warming are more pronounced during winter months (Fig. 2a). The global surface temperature signature of NA_c1 is depicted in Fig. 3. The strong warm anomaly off the coast of Newfoundland is due to a contraction of the SPG (described in more detail in section 3b) and the resulting northward migration of the Gulf Stream. The opposite sign anomalies in the Southern Ocean and parts of Antarctica are small in amplitude (about 0.5° – 1° C) compared to the changes around Greenland. This anticorrelation is suggestive of the “bipolar seesaw” (Stocker and Johnsen 2003) but is not analyzed here because of the small signal-to-noise ratio.

The tropical temperature difference between NA_c1 and NA_w1 is also small in amplitude compared to the high northern latitude changes, but has the same sign. Tropical Pacific precipitation changes associated with NA_c1 feature a dipole pattern (not shown) that corresponds to a precipitation decrease in the western Pacific warm pool (WPWP) and a simultaneous increase in the eastern tropical Pacific. This is consistent with paleoreconstructions that connect Greenland stadials with decreased precipitation over the WPWP and dominant El Niño-like conditions (Stott et al. 2002; based on magnesium/calcium composition and $\delta^{18}\text{O}$ of planktonic foraminifera).

The onset of the events based on Greenland temperature are years 326, 591, and 721 (e.g., Fig. 2, red lines).

TABLE 2. Heat and salinity budget (upper 280 m) of the Labrador Sea (53° – 65° N, 60° – 45° W) for the precooling phase during NA_w1 (years 270–290) and a phase after the first transition during NA_c1 (years 381–401). Furthermore two values are given for the transition period (years 310–320 and 320–330). The tendency term is averaged over the transition period. Negative signs imply a cooling and freshening of the box.

Budget term		Labrador Sea			
		Years 270–290	Years 310–320	Years 320–330	Years 381–401
Advection	Temperature (W m^{-2})	25.23	23.14	14.95	8.47
	Salt [10^{-8} kg m (kg s^{-1})]	10.43	10.45	9.21	7.84
Diffusion (including convection)	Temperature (W m^{-2})	60	48.54	52.7	9.86
	Salt [10^{-8} kg m (kg s^{-1})]	–10.29	–10.33	–9.06	–7.69
Surface flux	Temperature (W m^{-2})	–86	–72.45	–69.3	–18.87
	Salt [10^{-8} kg m (kg s^{-1})]	–0.15	–0.14	–0.16	–0.15
Tendency			Years 315–335		
	Temperature (W m^{-2})			–2.2	
	Salt [10^{-8} kg m (kg s^{-1})]			–0.016	

In the following section 3b we focus only on the first cooling event (year 326). The sequence of events leading to the abrupt warming (year 591) is briefly documented in section 3c. Section 3b describes the dynamics of the first climate transition based on the following sequence of events. A stochastic atmospheric circulation anomaly, resembling a strong negative North Atlantic Oscillation (NAO) phase is forcing a circulation anomaly in the SPG [section 3b(1)]. The SPG switches to a weak circulation mode due to a salinity driven positive feedback loop, shutting down deep water convection in the LS, and weakening the AMOC. Associated with the weaker circulation mode is a colder surface subpolar ocean [section 3b(2)]. As a consequence sea ice concentration increases in the LS, which in turn causes a reorganization of the atmosphere and a drop in Greenland temperature [section 3b(3)].

The atmospheric changes over the NA can thus be separated into two parts: an initial trigger that resembles a negative NAO phase and a positive sea ice–sea level pressure feedback, namely an anticyclonic anomaly that persists for about 200 years, and sustains the anomalous atmospheric forcing of the ocean.

b. Dynamical changes

1) ATMOSPHERIC TRIGGER—FROM YEAR 310 TO YEAR 320

In the beginning (years 310–315; Fig. 4a) an anticyclonic SLP anomaly evolves, centered between Greenland and northwestern Europe and resembling a negative NAO phase. The anticyclonic anomaly moves southwestward and decays over the next five years (Fig. 4b). The NAO is known to drive the dominant part of NA—in particular the LS—ocean heat transport variability, through changes in wind stress and buoyancy

forcing (e.g., Eden and Willebrand 2001). The total surface heat flux over the LS weakens at this point by about 14 W m^{-2} [difference between the first (years 270–290) and second column (years 310–320) in Table 2] as expected from a negative NAO phase (i.e., less heat loss of the LS to the atmosphere). The surface heat flux over the entire SPG region decreases as well, although the amplitude is small. At about the same time the wind stress curl north of the zero wind-curl line reduces (Fig. 5a, years 310–315, and Fig. 5b, years 315–320). At this point the maximum changes are located above the central and eastern SPG where they account for a 30%–50% reduction compared to the long-term mean. Furthermore the zero wind-curl line shifts farther north, contributing to a contraction of the SPG.

To estimate the importance of the changed wind stress curl in forcing the anomalous SPG circulation the Sverdrup transport was calculated according to Sverdrup theory (e.g., Pedlosky 1996). The Sverdrup transport in the LS and the northwestern NA is compared to the actual circulation changes in this region and the entire SPG (Fig. 6). The Sverdrup transport reproduces the anomalous SPG circulation well.

2) OCEAN AND SEA ICE RESPONSE—YEAR 315 ONWARD

The total difference NA_w1 – NA_c1 in the strength of the circulation [represented here by the barotropic streamfunction (BSF)] in the core region of the SPG accounts for about 10Sv, a 30% reduction (Fig. 7, contours). At the southern edge the circulation changes up to 20Sv due to a northward shift of the Gulf Stream path. The temperature of the upper central SPG decreases by up to 8°C in NA_c1 relative to NA_w1 (Fig. 7, colors).

At the onset of the first cooling transition the decreased wind stress curl forcing (year 310 onward; Figs. 5a,b) causes a first weakening of the SPG circulation

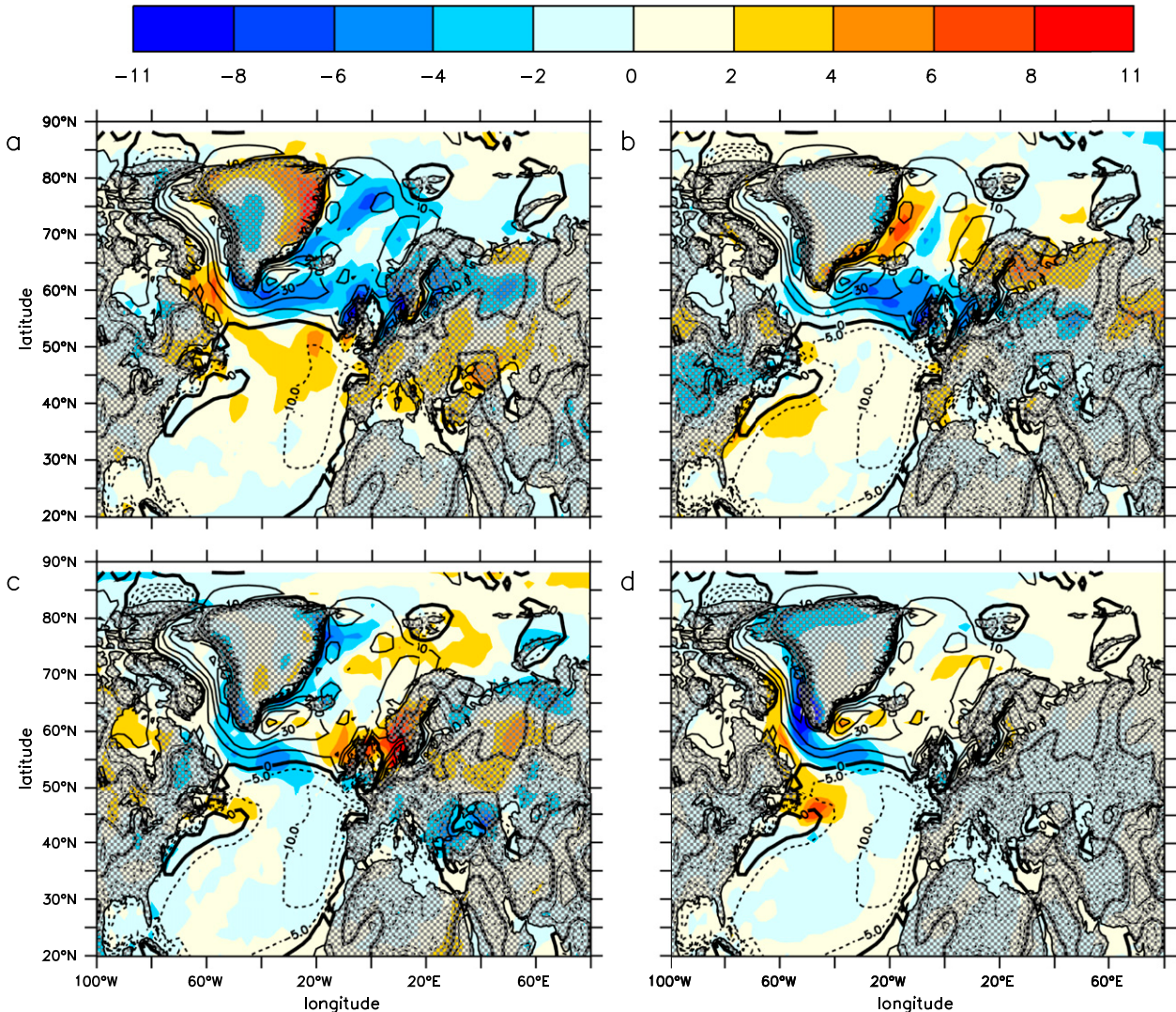


FIG. 5. Wind stress curl anomaly (10^{-8} N m^{-3}) for (a) years 310–315, (b) years 315–320, (c) years 320–325, and (d) NA_c1 (years 350–550). All anomalies are relative to NA_w1. Contours show the 1000-yr mean of wind stress curl.

(Fig. 6) around year 318. This time scale is in excellent agreement with the suggested time lag of 3 years after that the SPG strength reduces in response to wind stress curl changes associated with a negative NAO (Eden and Willebrand 2001). This weakening initiates a positive feedback loop in the SPG leading to the large ocean temperature (color) and circulation (contours) response depicted in Fig. 7. Figure 8a shows the density–depth evolution in the LS. Because of a drop in salinity of 1.6 psu (Fig. 9a; around year 319) the density in the upper LS starts to decrease simultaneously (year 319) with the declining gyre circulation. To understand the upper ocean salinity decrease in the LS, salinity budget terms for the upper almost 300 m of the LS are depicted in Fig. 10 and Table 2. Salinity advection decreases from

year 319 onward (because of advection changes through the southern and eastern face of the box), but this decrease is largely compensated by lower diffusion (including convection), which normally contributes to freshening of the LS. The tendency term becomes negative for a 20-yr period from year 315 onward (Table 2 and Fig. 10b), indicating the transition period, due to a negative balance of advection and diffusion. From about year 325 to year 335 the surface fluxes contribute to the negative tendency. Because the surface fluxes do not show a trend over the transition period, this indicates that the decrease of salinity in the LS and the entire SPG is a direct consequence of the slowdown of the SPG circulation. This is consistent with a model study by Born et al. (2013b), who show that salt

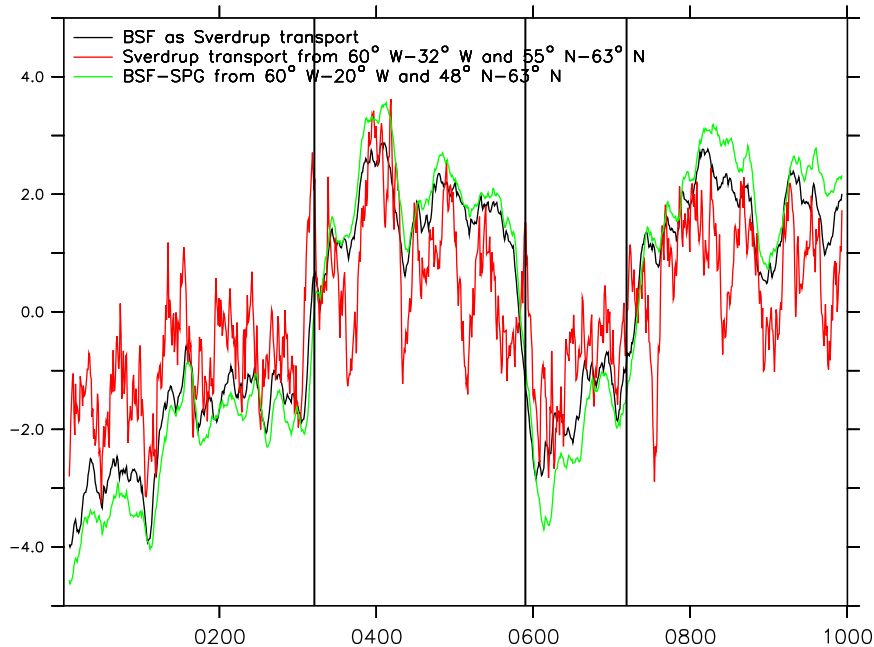


FIG. 6. Sverdrup transport anomaly (Sv) (red; averaged over 55° – 63° N, 60° – 32° W), actual circulation anomaly in the SPG (Sv) averaged over the same region as the Sverdrup transport (black), and over the entire SPG (green; 48° – 63° N, $\sim 20^{\circ}$ – 60° W). All time series are smoothed by a 15-yr running mean.

transport in the Irminger Current increases with a stronger circulation of the SPG, independent of salinity in the source region of the Irminger Current. They find that enhanced volume transport overcompensates possible low salinity anomalies in the source region by about two orders of magnitude. That implies a decreased salinity transport toward the LS and central parts of the SPG during periods of decreased gyre circulation. A decrease of salinity is seen in the entire water column of the LS (from 65° to 55° W; Fig. 9a) but with lower amplitude than at the surface.

As a result of the decreased surface density (Fig. 8a) the water column in the LS is stably stratified and maximum March mixed layer depth (MLD) reduces from year 319 onward (Fig. 8b). Eventually, during NA_c1 maximum March MLD is in average below 200 m, indicating no deep water convection. Slightly increased MLD south of Iceland (Fig. 11) indicates a minor compensation of deep water formation at this location during NA_c1. This is caused by a warm temperature anomaly at a depth of approximately 1300 m (Fig. 9b). The decrease in deep water convection in the LS causes a slowdown of the AMOC from around year 325 (maximum AMOC is located around a depth of 880 m and between 35° and 40° N; Fig. 8c). However, the AMOC does not shut down because of the still active deep water convection in the Nordic seas and the enhanced deep

water convection south of Iceland. The reduced horizontal density gradient between the center and the boundary current (cf. the stronger salt anomalies toward the west in Fig. 9a) weaken the gyre circulation further, thus closing the positive feedback loop (Born and Stocker 2014; Born et al. 2013a).

The cooling of the upper LS is a consequence of reduced convection and advection of temperature (both from year 320 on, column 2 of Table 2). There is a small warm anomaly (0.1° – 0.3° C; Fig. 9b) in the LS in the intermediate and deeper ocean during NA_c1. However, because of the still active deep water convection in the NA the warm anomaly never becomes strong enough to destabilize the water column and thus cannot trigger the onset of NA_w1, in contrast to what Dokken et al. (2013) find for the Nordic seas. The intermediate depth warming is more pronounced in lower latitudes (up to 45° N, not shown). In the Nordic seas the surface layer is fresher and colder during NA_c1. However, the warmer subsurface Atlantic inflow becomes colder and less saline too and a strong halocline is always sustained. This might be due to the enhanced deep water convection south of Iceland. Changes in thermohaline structure around Iceland (the Nordic seas) occur about 10 (30) years after the decrease in Greenland temperature sets in and thus most likely reflect the changed ocean circulation.

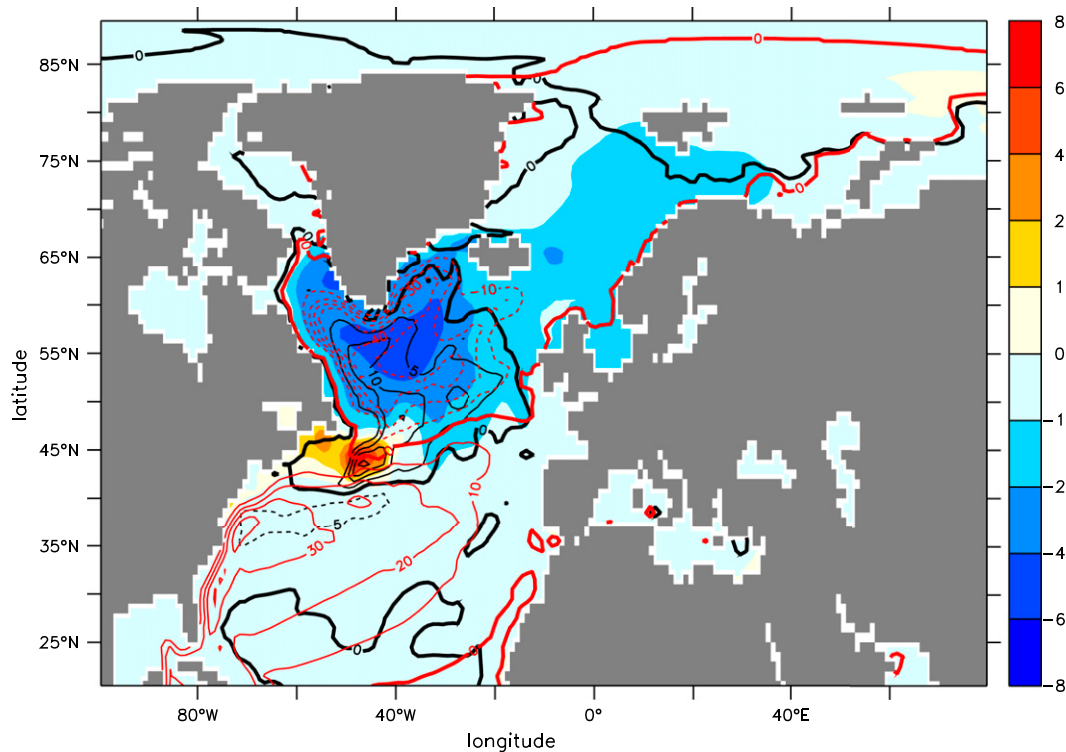


FIG. 7. Barotropic streamfunction anomaly (Sv; black contours) and temperature anomaly ($^{\circ}\text{C}$; colors) averaged over the upper 100 m in the subpolar gyre, difference between NA_c1 (years 350–550) and NA_w1 (years 50–250). Contour interval is 5 Sv; full lines show positive anomalies and dashed lines negative anomalies. The red contours show the 1000-yr mean of barotropic streamfunction (Sv). The contour interval is 10 Sv; full contours indicate anticyclonic and dashed contours cyclonic circulation.

In contrast to the LS the heat budget in the SPG box (not shown) is dominated by changes in temperature advection, due to a decrease of heat advected into the box through the south and from below, partly balanced by a decrease in heat advected through the north face. Diffusion and surface fluxes counteract the cooling tendency of the decreased advection, but are smaller in magnitude.

As a consequence of the colder ocean temperatures sea ice growth commences (from year 321 onward) in the LS. Annual maximum sea ice concentration, on average, increases here by about 100% relative to NA_w1, equivalent to about 30% increased sea ice concentration (Fig. 2b). The difference in horizontal extent of annual maximum sea ice concentration between NA_c1 and NA_w1 is depicted in Fig. 12. The changes are largest in the LS (up to a difference of 90% sea ice coverage) and stretch from there with lower amplitude along the southeastern coast of Greenland, north of Iceland toward Svalbard and until the northern coast of Norway. A similar spatial pattern of sea ice increase is observed at the northeastern coast of Asia (not shown) though smaller in amplitude. The sea ice edge progresses farther south and east in the Nordic seas and the LS as indicated

by the white and black contours in Fig. 12. The sea ice increase causes the surface heat fluxes in the LS to decrease dramatically (from year 322 onward). The changed surface heat fluxes partly balance the aforementioned cooling effect of decreased advection and convection. The transition in LS sea ice concentration takes about 80 years from warm to cold (years 326 and 719) and about 20 years from cold to warm (year 591; Fig. 2b). Both sea ice growth and retreat start in the LS region before spreading to the other regions. Additionally an increased sea ice cover weakens the SPG circulation through insulating it from wind stress forcing (Jochum et al. 2012).

3) ATMOSPHERE RESPONSE—YEAR 320 ONWARD

The reduced heat fluxes [reduced by about 70 W m^{-2} , difference between years 270–290 (column 1) and years 381–401 (column 4) in Table 2] above the LS (i.e., cooling of the atmosphere) are mainly a result of increased sea ice cover in the LS. They force a cold core high pressure anomaly, which sustains the anomalous forcing of the weakened gyre circulation. This atmospheric response starts to become apparent from years 320 to 325 (Fig. 4c).

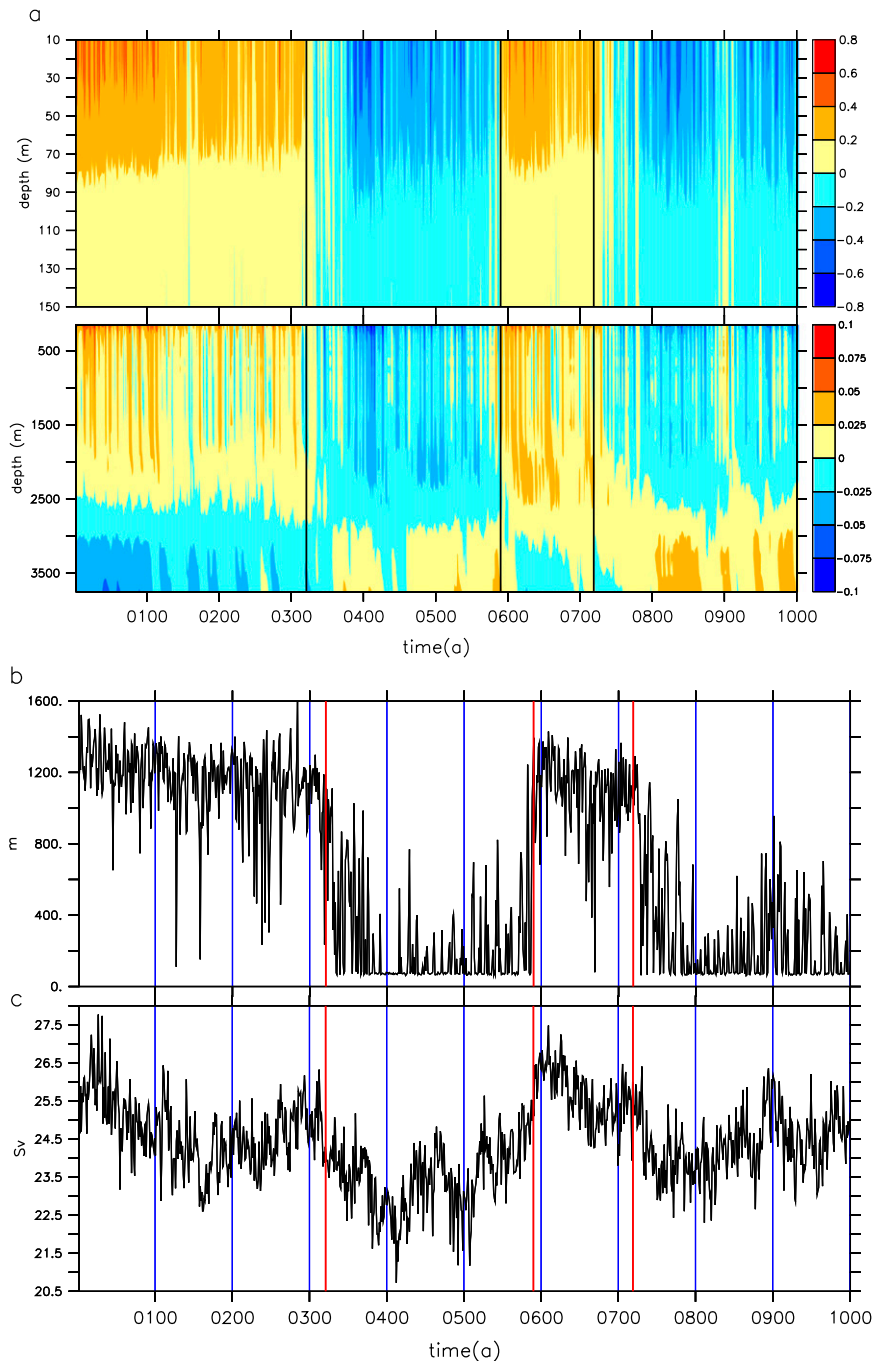


FIG. 8. (a) Density anomaly (kg m^{-3}) in the LS (averaged over about $55^{\circ}\text{--}63^{\circ}\text{N}$, $60^{\circ}\text{--}45^{\circ}\text{W}$) relative to the 1000-yr mean, (b) maximum March MLD (m) in the LS [same region as in (a)], and (c) maximum AMOC (Sv).

The anomaly strengthens in amplitude southwest of Greenland above the LS and extends, with reduced amplitude, far across the Asian continent. It persists for about 200 years (Fig. 4d) with an average spatial maximum of 2.8hPa above the LS. Associated with this

also a persistent localized decrease in wind stress curl (Fig. 5d) during NA_c1. The largest changes occur west off Greenland where the wind stress curl reduces to about 70% of its original magnitude (NA_w1) and to about 60% of its original magnitude across central parts of the SPG.

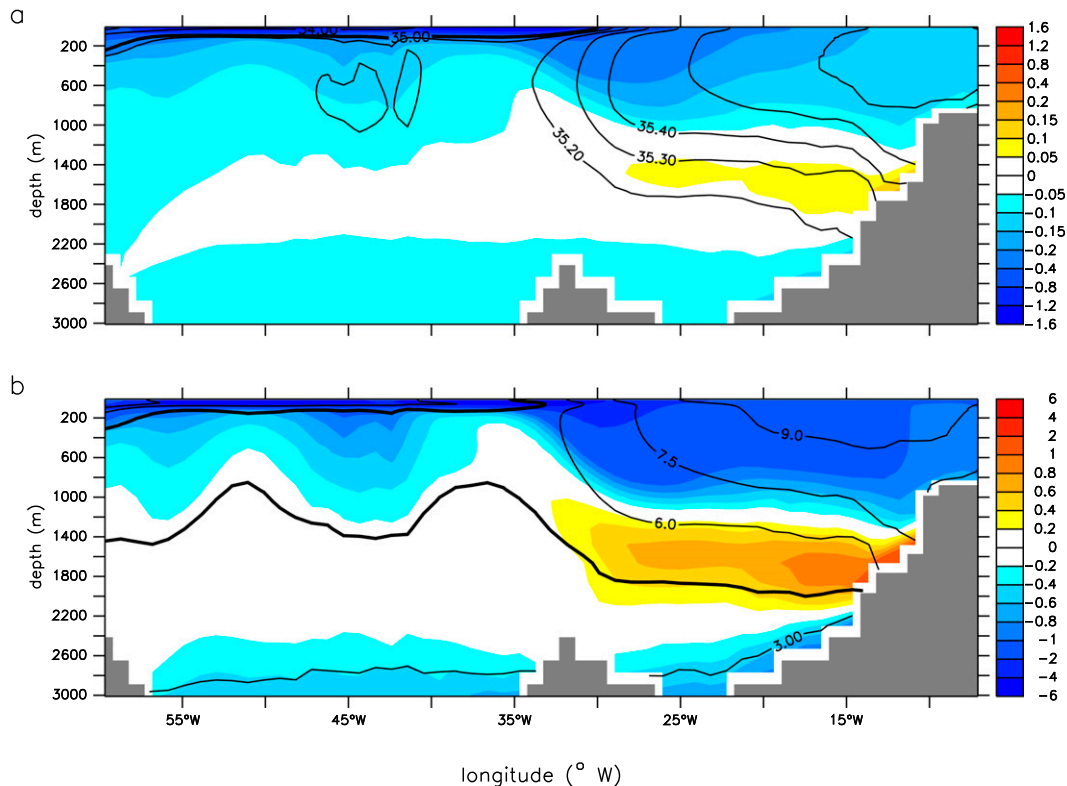


FIG. 9. (a) Salinity (psu) and (b) temperature ($^{\circ}\text{C}$) anomaly in a cross section through the SPG averaged from about 57° – 61°N . Anomaly is between NA_c1 and NA_w1. Contours show the 1000-yr mean and the intervals are 1 psu from 33 to 35 psu and 0.1 psu from 35 to 35.6 psu in (a) and 1.5°C in (b).

This response of atmospheric circulation to sea ice anomalies was demonstrated by Deser et al. (2007) on shorter time scales (i.e., over one winter–spring season). This is a directly forced baroclinic response and opposite in sign to the equivalent barotropic response to positive (negative) SST anomalies, which is invoked to explain the evolution of negative (positive) NAO phases (e.g., Farneti and Vallis 2011). The equivalent barotropic response is fully established after 2–2.5 months (Deser et al. 2007) and dominates the overall response. However, in our case the anomalous surface heat fluxes, forcing the anticyclonic anomaly, persist during the entire NA_c1 because of the involved ocean circulation and sea ice changes.

Eventually the sea ice concentration changes cause the drop in Greenland temperature (from year 326 onward) by insulating the atmosphere from the ocean heat reservoir as suggested by Li et al. (2005) and Li et al. (2010).

c. Warming event

The SLP anomaly decreases for the first time around year 500 but remains then for another almost 80 years

in a slightly lower but stable state. Around year 580 a cyclonic SLP anomaly evolves centered off northern Norway (Fig. 13a, years 578–583). From here the cyclonic center moves to the central Arctic Ocean around year 585 (Fig. 13b, years 584–589), slowly displacing the remaining anticyclonic SLP anomaly at the southern tip of Greenland (Fig. 13c, years 589–594). This SLP anomaly (Figs. 13a,b) resembles closely the anomaly that evolved beside the anticyclone above Greenland in DO_a and DO_b (green and red curve in Fig. 1) and appeared to hinder the full amplitude of changes to evolve in DO_a and DO_b. Finally SLP drops abruptly to its preevent value between year 595 and 600 (cf. Figs. 4d and 13d). The surface heat fluxes in the LS and SPG change around year 587 and 590 respectively, while the Sverdrup transport features to high interannual variability to determine smaller trends previous to a sudden jump back to the precooling state at around year 595 (Fig. 6). The SPG gyre circulation changes around year 583 and sea ice concentration (Fig. 2b) and temperature above the LS follow at year 585 (Fig. 14). In Fig. 14 the temperature evolution at different locations across Greenland are compared to changes in temperature above the LS. Compared to

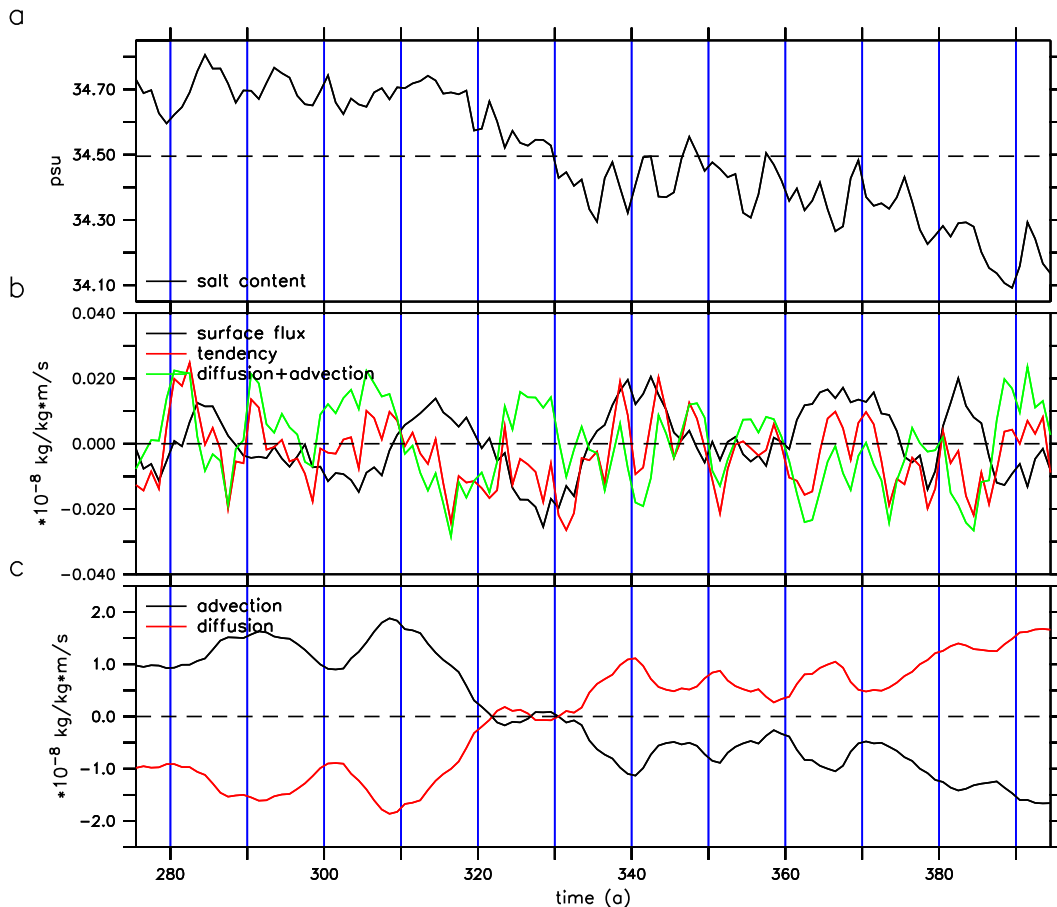


FIG. 10. Salinity budget for the upper 280 m of the LS (53° – 65° N, 60° – 45° W) over the transition between NA_wl and NA_c1. (a) Salinity content (psu); (b) surface flux anomaly (black), tendency term (red) and combined diffusion and advection anomaly (green); and (c) advection anomaly (black) and diffusion anomaly (red). All budget term time series are smoothed by a 7-yr running mean.

the original amplitude above the LS of about 8°C the amplitude of annual mean temperature change is reduced to approximately 2° – 3°C at different points at Greenland. The warming too is more pronounced during winter months (cf. annual minimum temperature in Fig. 2). It also becomes apparent from Fig. 14 that the signal transmission from the LS to northern Greenland takes about 5–10 years. Thus Greenland temperature increases abruptly from around year 591.

In general the warming and the cooling event feature the same sequence of events, that is, atmospheric circulation changes [SLP, surface heat flux, and wind stress (only determinable for the cooling transition)] followed by SPG circulation changes and eventually a change in sea ice concentration in the LS followed by changes in Greenland temperature. This raises the question why the transitions, at least in Greenland temperature, feature an asymmetric pattern. This question is

not addressed in detail but possible causes are discussed in section 4.

d. Dependence on the climatic background state—A comparison to the HI preindustrial control simulation

The question arises why such spontaneous climate transitions do not occur in the vast majority of state-of-the-art GCM runs (see section 1). In the following section we thus address this question in terms of the dependence of the above described mechanism on the climatic background state; in particular, the differences of HI and CONT in the NA are compared. Both runs are set up with the same external boundary conditions and only differ in the resolution of the atmosphere. However, the mean states of ocean and atmosphere are different. The following numbers refer to a comparison between the ocean and atmosphere state in the NA in a 50-yr average directly previous to the first transition and

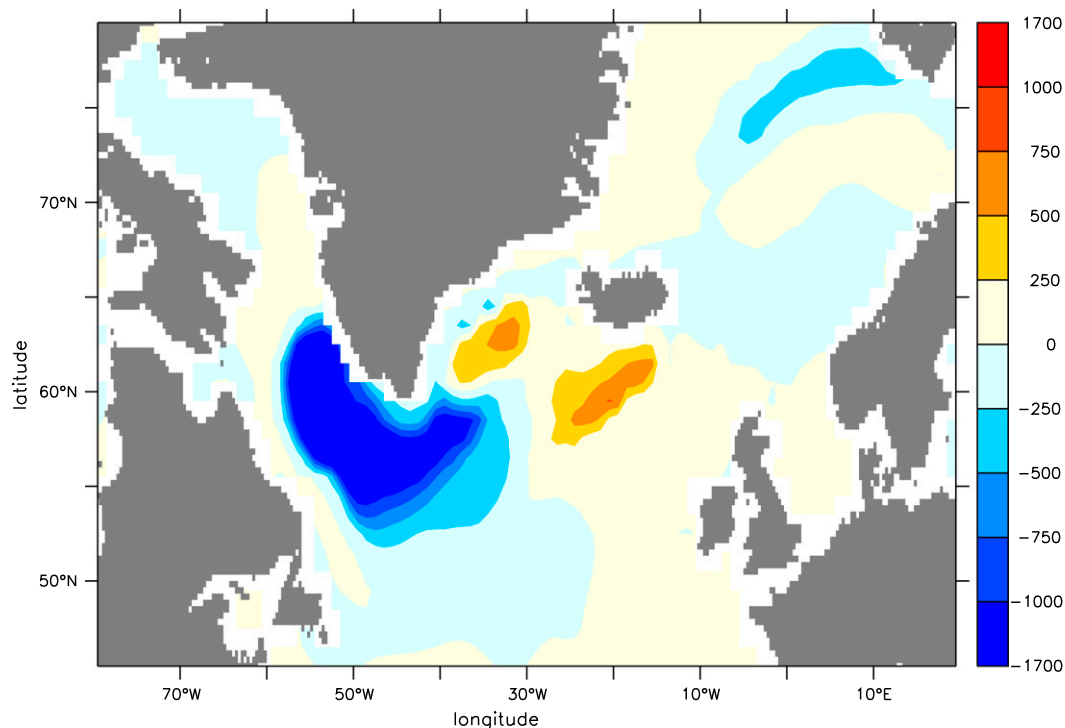


FIG. 11. March maximum MLD (m) anomaly between NA_c1 and NA_w1.

the same time period in HI. To begin with HI features a warmer SPG (about $0.5^{\circ}\text{--}2^{\circ}\text{C}$) and a more saline western SPG (about $0.3\text{--}0.6$ psu) and is slightly less saline in the eastern SPG (about 0.1 psu). These differences alone have some implications for the proposed positive feedback mechanism in the SPG. The effect of salinity anomalies on the density of water is larger for colder temperatures. Thus in HI higher salinity advection anomalies would be necessary to initiate the described positive feedback loop, including the shutdown of deep water formation in the LS. Moreover the western SPG is already less saline in CONT and thus a smaller salinity advection anomaly can already cause the stabilization of the LS water column. Second, the circulation in the SPG is weaker in CONT and thus also favors a switch to a weak circulation mode. Furthermore, the atmospheric mean state over the NA is distinctly different in the two simulations. The Icelandic low is more pronounced in HI, with a lower mean SLP of about 2 hPa. Figure 15 reveals stronger SLP gradients between the Icelandic low and Azores high in HI than in CONT. A smaller SLP anomaly in CONT thus weakens the gradients between the Icelandic low and Azores high sufficiently to trigger the aforementioned changes in wind stress curl and thus eventually the ocean circulation changes. Compared to NCEP reanalysis data (Kalnay et al. 1996) from 1948 until 2014, HI seems to overestimate the

gradients, whereas CONT agrees well (HI and CONT are preindustrial control simulations). The spread of both distributions seems to be realistic. Finally, CONT features stronger ENSO variability than HI and present-day observations (Shields et al. 2012, their Fig. 17).

e. Ocean–sea ice experiments with anomalous atmospheric forcing—Testing the trigger

To test the above proposed mechanism and to infer more details about the atmospheric circulation anomaly and the relative importance of buoyancy and wind stress forcing of the SPG circulation anomaly, several OI simulations are conducted (section 2). In Fig. 16 the annual maximum sea ice concentration in the LS is depicted as an indicator of the climate transitions. Simulations OI_a through OI_d feature rapid increasing sea ice concentration (Fig. 16c), while OI_e and OI_f show a decrease in sea ice concentration (Fig. 16b) where the later one was started from ocean sea ice conditions of the red curve experiment (i.e., from a high sea ice concentration state).

For the longest experiment (OI_b; Fig. 16c, red curve) the circulation change of the SPG (not shown) and the MLD in the LS (not shown) between the five first and last years of the simulation were compared. The MLD in the LS decreases by about 240 m and the circulation changes in the core region of the SPG account for about

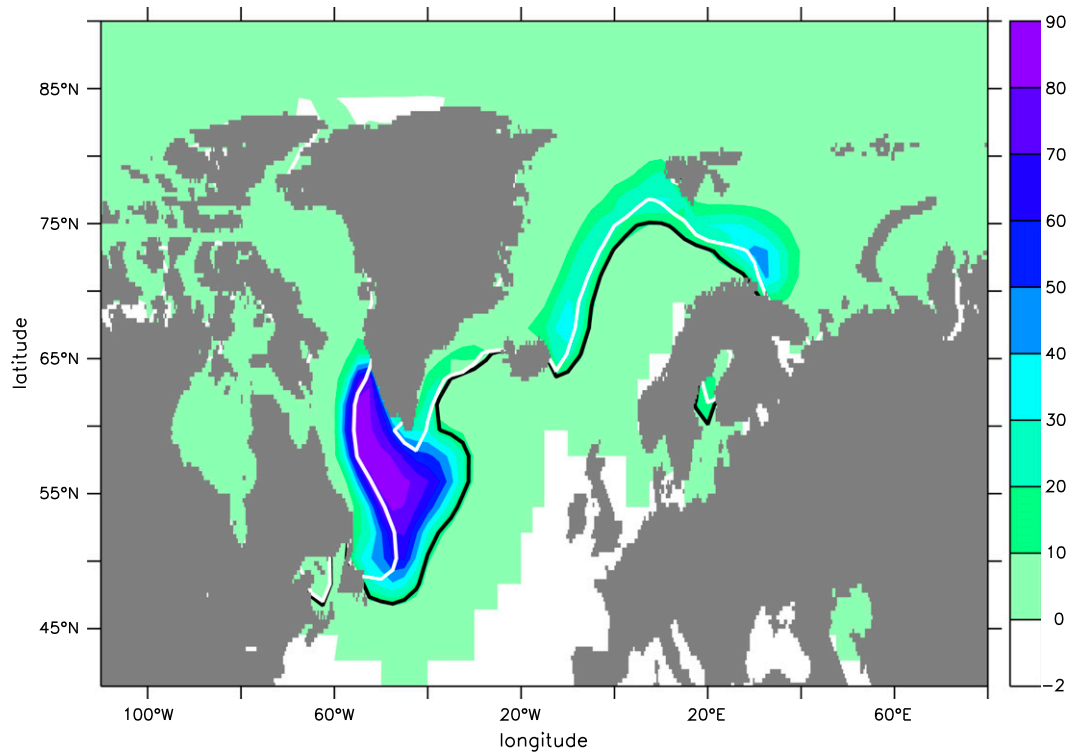


FIG. 12. Difference in annual maximum sea ice concentration (%) between NA_c1 and NA_w1. Overlying contours show the averaged annual maximum sea ice extent (15%) for NA_c1 (black) and NA_w1 (white).

6 Sv—a value similar to the 10 Sv in CONT. Thus the experiments seem not only to reproduce the changes in sea ice concentration, but as well the ocean circulation changes.

4. Discussion

Based on the scenario above, three topics deserve further attention:

- stochastic forcing,
- tropical–extratropical atmospheric connections, and
- dependence on background climate state.

a. Stochastic forcing

We tested the proposed mechanism by forcing OI experiments with atmospheric fluxes extracted from CONT and starting from ocean and sea ice conditions of HI. That these simulations reproduce not only the same changing sea ice concentration but also the same changes in ocean circulation gives us confidence in the aforementioned mechanism. This sensitivity to stochastic forcing raises the question of what forces the SPG in the real world. Unfortunately there is still no consensus on whether buoyancy (e.g., Yeager and Danabasoglu 2014; Eden and Jung 2001) or wind forcing

(e.g., Eden and Willebrand 2001; Häkkinen et al. 2011) dominates in determining the strength of the SPG circulation. This depends as well on the considered time scales, with a faster response time to altered wind stress forcing. We showed additionally that the SLP gradients between the Icelandic low and Azores high in CONT are weaker than in HI. Thus a smaller stochastic anomaly in CONT can trigger the atmosphere and ocean circulation changes.

Rearrangements in the steady atmospheric circulation pattern and the transient eddy activity above the NA occur during the last glacial period (e.g., Li and Battisti 2008). The primary cause for these differences in atmospheric circulation is ice sheet topography, in particular the Laurentide ice sheet (e.g., Pausata et al. 2011). The absence of ice sheet topography-driven atmospheric circulation changes could thus also explain why D-O cycles do not occur during the Holocene (see e.g., Wunsch 2006). There is evidence from observations that atmospheric rearrangements occur prior to Greenland temperature changes. Deuterium excess shows that Greenland precipitation sources change 1–3 years before Greenland air temperature (Steffensen et al. 2008). Change of moisture source region implies an abrupt change of the local atmospheric circulation or the

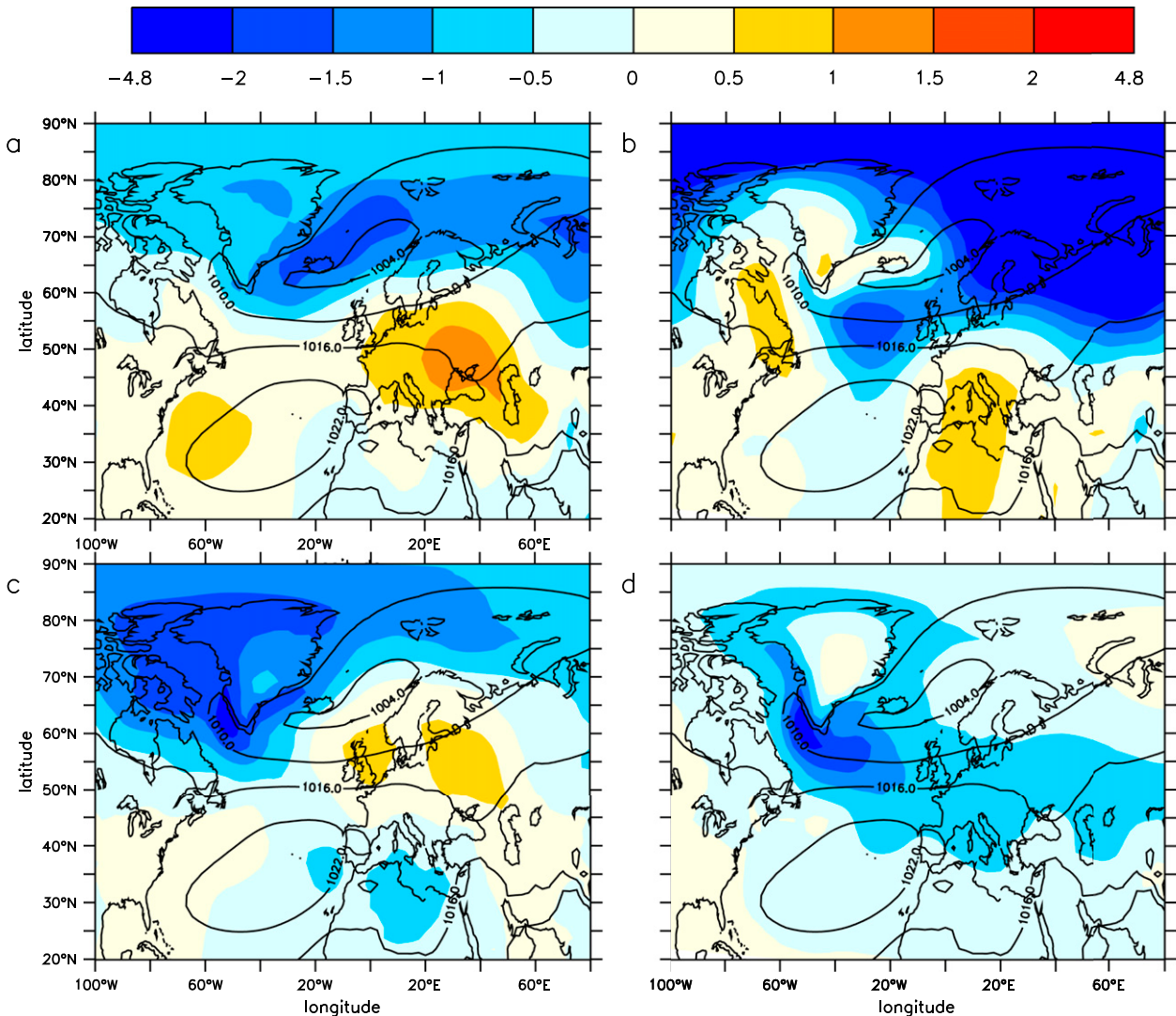


FIG. 13. Sea level pressure anomaly (hPa) for (a) years 578–583, (b) years 584–589, (c) years 589–594, and (d) the second warm phase (years 600–700). All anomalies are relative to NA_c1 and negative values imply a lower SLP than during NA_c1. Contours show the 1000-yr mean of SLP.

opening of a new source (e.g., by changing from sea ice covered to open ocean). Both changes are seen in CONT: we find atmospheric rearrangements over the NA prior to the abrupt temperature change. In addition, the sea ice cover and temperature changes in the LS lead the temperature signal in Greenland (Fig. 14) and thus establish or remove a possible Greenland precipitation source.

Additionally the ^{231}Pa and ^{230}Th reconstructions by Böhm et al. (2015) suggest that a strong AMOC prevailed during most parts of the last glacial period and shutdown of the AMOC occurred only during Heinrich events close to LGM. This view is supported by our findings, which provide a mechanism for abrupt Greenland climate shifts without strong AMOC variations.

An interesting aspect of the atmospheric response is that it might contribute to the sawtooth shape of the Greenland temperature signal. Deser et al. (2004) and Deser et al. (2007) find that decreased sea ice concentration (or warmer SST) causes a cyclonic anomaly stronger in amplitude than the anticyclonic anomaly forced by increased sea ice concentration (colder SSTs). Thus larger changes in sea ice cover and temperature are necessary to build up the anticyclonic anomaly than decreasing it again.

However, Deser et al. (2004) and Deser et al. (2007) are based on atmosphere model simulations with prescribed SST and sea ice extent anomalies from observed trends. Feedbacks on the SST and sea ice anomalies can thus only be estimated by a comparison of the observed

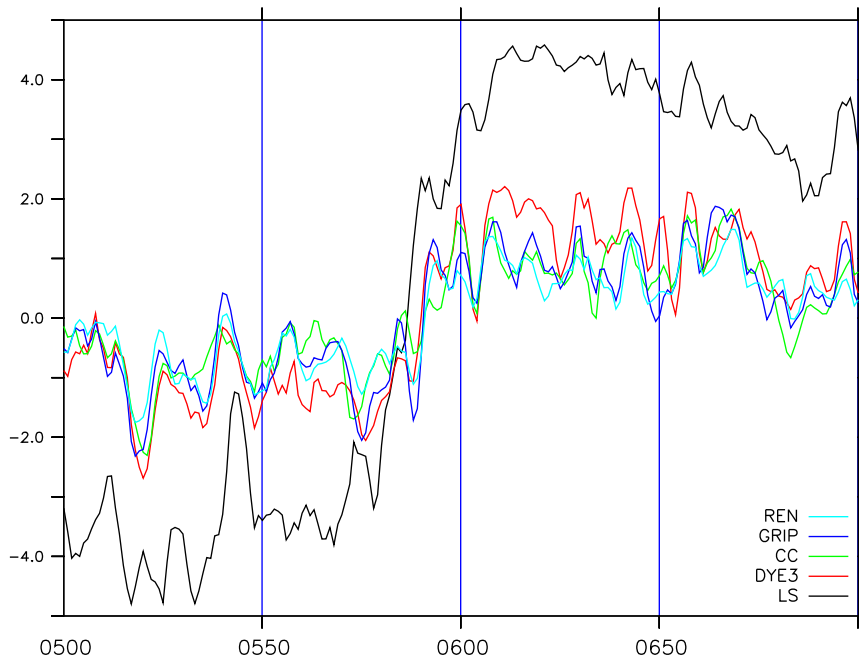


FIG. 14. Annual mean temperature anomaly (relative to 1000-yr mean) over the warming transition for the LS (55° – 65° N, 50° – 60° W; black) and different grid points approximately corresponding to different ice core locations at Greenland: Renland (REN) in cyan, Greenland Ice Core Project (GRIP) site in blue, Camp Century (CC) in green, and Dye-3 site (DYE3) in red. All time series are smoothed by a 5-yr running mean.

atmospheric trends and the atmospheric response in their simulations; they estimate the feedback to be negative but weak.

b. Tropical–extratropical connections

The initial change in SLP is in the range of natural variability, thus no further trigger is needed to explain the occurrence of the stochastic atmospheric anomaly over the NA. In the extratropics, El Niño–Southern Oscillation (ENSO) variability is known to alter, in particular, the likelihood of extreme pressure events to occur (e.g., Sardeshmukh et al. 2000; Palmer 1993). Therefore in the following section we discuss changes in temperature and precipitation in the tropical Pacific and possible connections with the anomalous NA atmospheric circulation.

For all three transitions (from warm to cold: years 326 and 719; from cold to warm: first changes at year 550; and finally back to initial state around year 590) changes in tropical precipitation occur simultaneously or previous to the changes in SLP over the NA (Fig. 17). Teleconnections from tropics to extratropics work virtually instantaneously, whereas a signal transferred inversely takes about 2–3 years (Chiang and Bitz 2005). Two other strong increases in precipitation at around year 350 and 890 are both followed by a weakening of

the anticyclone and a temporary drop in sea ice concentration (cf. Fig. 2). Furthermore, temperatures in the WPWP are anomalously warm for about 20–30 years previous to the two cooling events. The shifts in tropical atmospheric deep convection associated with SST changes generate planetary waves that modify global patterns of SLP (e.g., Sardeshmukh and Hoskins 1988). It is difficult to associate unambiguously particular sea level pressure changes with particular convection changes (Ting and Sardeshmukh 1993), but the present SLP differences between NA_c1 and NA_w1 are quite similar to pressure differences induced by El Niño teleconnections (e.g., Trenberth et al. 1998), in particular a weakening of the pressure difference between the Azores and Iceland. A modeling study by Merkel et al. (2010) shows altered ENSO teleconnections during past glacial climates. They demonstrate that teleconnections into the NA were strong during preindustrial times (not shown, but also true for CONT) and Greenland interstadials, while there were weak or no teleconnections during the LGM, Heinrich stadial 1, and Greenland stadials (see Fig. 11 in Merkel et al. 2010). Furthermore different ENSO variability is expected with different orbital forcing as also demonstrated by a modeling study of Timmermann et al. (2007). Paleoreconstructions showed that ENSO was at work over past glacial

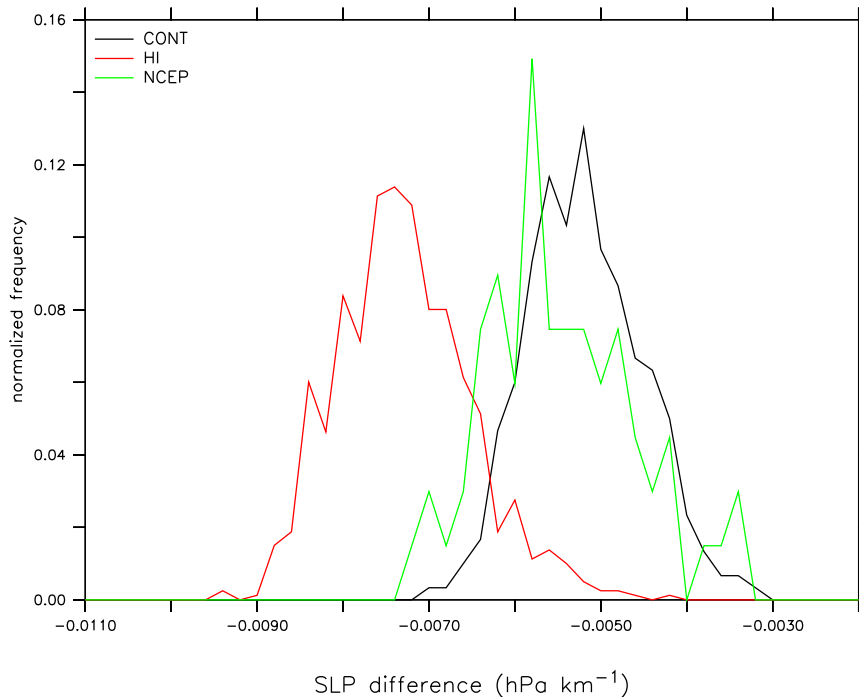


FIG. 15. Comparison of normalized annual SLP gradient distribution (hPa km^{-1}). The SLP gradient is calculated between subtropical high and subpolar low in the Atlantic for NCEP present-day reanalysis (green), CONT (black), and HI (red).

climates (e.g., Tudhope et al. 2001). Whether the strength was weaker, stronger, or not altered at all during past glacial climates is still debated. Whether the suggested tropical changes are a plausible scenario for D-O cycles depends thus upon better paleoreconstructions of altered ENSO strength and variability and its relative timing to Greenland ice cores.

As described in section 4a, there is also evidence for abrupt climate shifts in the NA under Holocene conditions (e.g., Bond et al. 1997). The modeling study by Liu et al. (2014), consistent with most paleo-ENSO reconstructions, describes an orbitally induced strengthening of ENSO during the Holocene epoch relative to the deglaciation. Moy et al. (2002), based on a Laguna sediment record in southern Ecuador, reconstruct millennial-scale variability of ENSO during the Holocene.

c. Dependence on background climate state

As mentioned previously, no further transitions between NA cold and warm phases occur in a 200-yr extension of this simulation, implying that the last cold state lasts for at least 400 years. This points toward a strong dependence on the climatic background state for the full chain of aforementioned processes to evolve. The analyzed simulation has a warm bias in global average,

but a cold bias in the NA and drifts toward a colder state. The ocean loses heat at -0.09 W m^{-2} over the last 600 years (Shields et al. 2012). Furthermore the NA (20° – 70°N) becomes more saline at intermediate depth while the upper NA ($\leq 500 \text{ m}$) becomes less saline, which has a stabilizing effect for the cold phase as stronger salinity anomalies are necessary for deep water convection to resume. We discussed in section 3d the differences between HI and CONT and how these differences promote the positive feedback loop in SPG circulation, salinity advection and deep water convection intensity as well as the probability of the triggering SLP anomaly to occur. CONT represents in several aspects a climate that is biased toward a glacial climate (e.g., temperature of the SPG).

The reproducibility of the transitions together with their occurrence at different points in time compared to the original simulation indicates that no long-term memory effects are necessary for the abrupt transitions to occur. Hence it supports our hypothesis that rather quasi-stochastic atmospheric forcing triggers a switch in a per se unstable ocean circulation regime, the strong and weak SPG circulation modes. It would be thus very interesting to analyze a parameter space (mainly of temperature and salinity) for which the SPG can flip. Born and Stocker (2014) show that a simple four-box

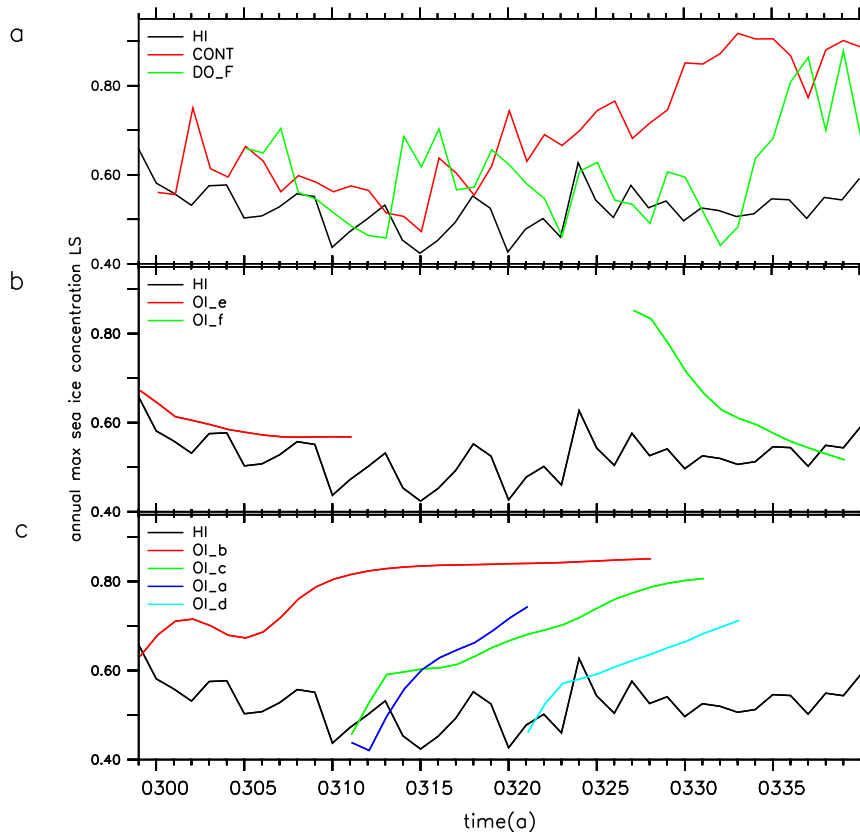


FIG. 16. (a) Annual maximum sea ice concentration in the LS (averaged over about 50° – 67° N, 63° – 40° W), in fully coupled simulations HI (black), CONT (red), and DO_F (green). (b) As in (a), but for the declining sea ice concentration OI experiments (using atmospheric fluxes of year 305/306 from DO_F). (c) As in (a), but for increasing sea ice concentration OI runs. For increasing sea ice concentration OI runs different years of atmospheric forcing from DO_F were tested: year 312/313 (OI_b, red; OI_c, green; and OI_d, cyan) and year 332/333 (OI_a, blue). As a reference HI is also shown in (b) and (c). See Table 1 for experimental setup of simulations.

model of the SPG is bistable. However, in reality and in a fully coupled climate model the parameter space would be more complex (i.e., ocean–atmosphere and ocean–sea ice feedbacks). How representative this simple model is for the real SPG remains unclear, but for our argumentation it is sufficient that the SPG is sensitive to small perturbations.

The dependence of the oscillations on the mean state of the SPG is an obvious drawback. The present mechanism should thus be evaluated under MIS3 conditions.

5. Summary

D-O-like transitions in Greenland temperature are found in a free CCSM4 integration and analyzed. It is notoriously difficult to establish cause and consequence in fully coupled simulations. With this caveat in mind we

suggest that the climate transitions are triggered by a stochastic change in SLP pattern over the NA. This state is associated with a weakened wind stress curl over the SPG. Consequently the gyre circulation slows down and advects less warm and saline subtropical waters to high latitudes, initiating a positive feedback loop toward a persistent weaker state of the SPG circulation and deep water convection in the LS. Sea ice growth commences in the LS due to locally reduced warm water transport and decreased ocean–atmosphere heat flux. The sea ice anomaly here allows for a cold core high to develop at the southwestern tip of Greenland and sustains the anomalous SLP pattern for about 200 years, the entire cold NA phase. The decreased deep water convection leads furthermore to a reduced AMOC of about 3–4 Sv and thus a further reduction in northward heat transport. The onset of the warming is initiated by a stronger Icelandic low and thus by removing the anomalous

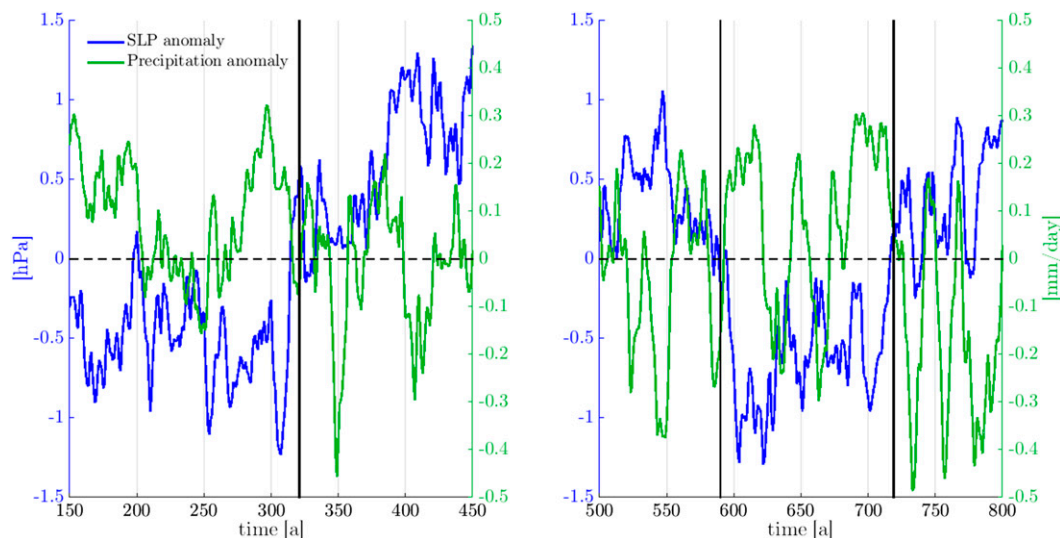


FIG. 17. Precipitation anomaly (mm day^{-1}) in the western tropical Pacific, averaged over 8°S – 8°N , 100°E – 180° , in green and sea level pressure anomaly (hPa) over the NA, averaged over 50° – 65°N , 50° – 20°W , in blue. Both time series are smoothed with a running mean over 10 years. (left) The first cooling event around year 326 and (right) the abrupt warming and the second cooling event around years 591 and 721, respectively.

atmospheric forcing the SPG circulation recovers, deep water convection resumes, sea ice cover retreats and Greenland temperature rises abruptly. The possible influence of tropical precipitation anomalies on the NA atmospheric trigger is discussed.

The present coupling between SPG, sea ice, and the Icelandic low has already been hypothesized by Seager and Battisti (2007). The central role of the sea ice has already been discussed by Li et al. (2005), although the mechanism causing a sudden sea ice retreat remains unclear. We have now identified a possible cause for sea ice changes: stochastic atmospheric forcing. The initial trigger of the transitions occurring herein and in Drijfhout et al. (2013) are in both cases stochastic atmospheric circulation anomalies. Additionally, the persistent anticyclonic anomalies above the NA during the cold event are alike. However the mechanisms sustaining this persistent anomaly are different. While Drijfhout et al. (2013) attributes the persistent anomaly to sea ice–atmosphere interactions later on amplified by ocean circulation feedbacks (mostly AMOC), we find that the changed oceanic gyre circulation plays a key role. Even though we see changes in thermohaline properties in the Nordic seas and the LS we find no evidence for the mechanism suggested by Dokken et al. (2013). Note, though, that the climate state of CONT is likely to be far from MIS3.

The present results are a promising starting point into the dynamics behind D–O cycles. To us it appears that their most critical and uncertain component is their

sensitivity to the NA background state and the structure of atmospheric noise that is needed to trigger a switch in the SPG state. Thus, we plan to continue our work with three complementary approaches: first, to constrain the mean state of the SPG as well as timing and nature of atmospheric circulation changes during MIS3 with paleoproxies; second, to perform more idealized GCM studies in which we can control background state and atmospheric noise; and third, to set up a full MIS3 simulation with the Community Earth System Model (CESM).

Acknowledgments. We are grateful to Matthew Long and Keith Lindsay for helping set up the ocean–ice simulations. Further we thank Andreas Born and Gokhan Danabasoglu for their insightful comments. We thank Sybren Drijfhout and two anonymous reviewers for the constructive comments that helped to significantly improve this study. NCEP reanalysis data are provided by the NOAA/OAR/ESRL PSD, Boulder, Colorado, from their website (<http://www.esrl.noaa.gov/psd/>). Computing resources were provided by the Climate Simulation Laboratory at NCAR’s Computational and Information Systems Laboratory, sponsored by the National Science Foundation and other agencies. The research leading to these results has received funding from the European Research Council under the European Community’s Seventh Framework Programme (FP7/2007–2013)/ERC Grant Agreement 610055 as part of the Ice2Ice project.

REFERENCES

- Andersen, K. K., and Coauthors, 2006: The Greenland ice core chronology 2005, 15–42 ka. Part 1: Constructing the time scale. *Quat. Sci. Rev.*, **25**, 3246–3257, doi:10.1016/j.quascirev.2006.08.002.
- Antonov, J., and Coauthors, 2010: *Salinity*. Vol. 2, *World Ocean Atlas 2009*, NOAA Atlas NESDIS 69, 184 pp.
- Arz, H. W., F. Lamy, A. Ganopolski, N. Nowaczyk, and J. Pätzold, 2007: Dominant Northern Hemisphere climate control over millennial-scale glacial sea-level variability. *Quat. Sci. Rev.*, **26**, 312–321, doi:10.1016/j.quascirev.2006.07.016.
- Barbante, C., and Coauthors, 2006: One-to-one coupling of glacial climate variability in Greenland and Antarctica. *Nature*, **444**, 195–198, doi:10.1038/nature05301.
- Bethke, I., C. Li, and K. H. Nisancioglu, 2012: Can we use ice sheet reconstructions to constrain meltwater for deglacial simulations? *Paleoceanography*, **27**, PA2205, doi:10.1029/2011PA002258.
- Böhm, E., and Coauthors, 2015: Strong and deep Atlantic meridional overturning circulation during the last glacial cycle. *Nature*, **517**, 73–76, doi:10.1038/nature14059.
- Bond, G., and Coauthors, 1997: A pervasive millennial-scale cycle in North Atlantic Holocene and glacial climates. *Science*, **278**, 1257–1266, doi:10.1126/science.278.5341.1257.
- Born, A., and T. F. Stocker, 2014: Two stable equilibria of the Atlantic subpolar gyre. *J. Phys. Oceanogr.*, **44**, 246–264, doi:10.1175/JPO-D-13-073.1.
- , —, C. C. Raible, and A. Levermann, 2013a: Is the Atlantic subpolar gyre bistable in comprehensive coupled climate models? *Climate Dyn.*, **40**, 2993–3007, doi:10.1007/s00382-012-1525-7.
- , —, and A. B. Sandø, 2013b: Coupling of eastern and western subpolar North Atlantic: Salt transport in the Irminger Current. *Ocean Sci. Discuss.*, **10**, 555–579, doi:10.5194/osd-10-555-2013.
- Broecker, W. S., G. Bond, M. Klas, G. Bonani, and W. Wolfli, 1990: A salt oscillator in the glacial Atlantic? 1. The concept. *Paleoceanography*, **5**, 469–477, doi:10.1029/PA005i004p00469.
- Cappelen, J., 2013: Greenland-DMI historical climate data collection 1873–2012—With Danish abstracts. DMI Tech. Rep. 13-04, 75 pp. [Available online at <http://www.dmi.dk/laer-om/generelt/dmi-publikationer/2013/>.]
- Chiang, J. C. H., and C. M. Bitz, 2005: Influence of high latitude ice cover on the marine intertropical convergence zone. *Climate Dyn.*, **25**, 477–496, doi:10.1007/s00382-005-0040-5.
- Cunningham, S. A., and Coauthors, 2007: Temporal variability of the Atlantic meridional overturning circulation at 26.5°N. *Science*, **317**, 935–938, doi:10.1126/science.1141304.
- Danabasoglu, G., S. C. Bates, B. P. Briegleb, S. R. Jayne, M. Jochum, W. G. Large, S. Peacock, and S. G. Yeager, 2012: The CCSM4 ocean component. *J. Climate*, **25**, 1361–1389, doi:10.1175/JCLI-D-11-00091.1.
- , and Coauthors, 2014: North Atlantic simulations in coordinated ocean-ice reference experiments phase II (CORE-II). Part I: Mean states. *Ocean Modell.*, **73**, 76–107, doi:10.1016/j.ocemod.2013.10.005.
- Dansgaard, W., and Coauthors, 1993: Evidence for general instability of past climate from a 250-kyr ice-core record. *Nature*, **364**, 218–220, doi:10.1038/364218a0.
- Deser, C., G. Magnusdottir, R. Saravanan, and A. Phillips, 2004: The effects of North Atlantic SST and sea ice anomalies on the winter circulation in CCM3. Part II: Direct and indirect components of the response. *J. Climate*, **17**, 877–889, doi:10.1175/1520-0442(2004)017<0877:TEONAS>2.0.CO;2.
- , R. A. Tomas, and S. Peng, 2007: The transient atmospheric circulation response to North Atlantic SST and sea ice anomalies. *J. Climate*, **20**, 4751–4767, doi:10.1175/JCLI4278.1.
- Dijkstra, H. A., 2007: Characterization of the multiple equilibria regime in a global ocean model. *Tellus*, **59A**, 695–705, doi:10.1111/j.1600-0870.2007.00267.x.
- Dokken, T. M., K. H. Nisancioglu, C. Li, D. S. Battisti, and C. Kissel, 2013: Dansgaard–Oeschger cycles: Interactions between ocean and sea ice intrinsic to the Nordic seas. *Paleoceanography*, **28**, 491–502, doi:10.1002/palo.20042.
- Drijfhout, S., E. Gleeson, H. A. Dijkstra, and V. Livina, 2013: Spontaneous abrupt climate change due to an atmospheric blocking–sea-ice–ocean feedback in an unforced climate model simulation. *Proc. Natl. Acad. Sci. USA*, **110**, 19 713–19 718, doi:10.1073/pnas.1304912110.
- Eden, C., and T. Jung, 2001: North Atlantic interdecadal variability: Oceanic response to the North Atlantic Oscillation (1865–1997). *J. Climate*, **14**, 676–691, doi:10.1175/1520-0442(2001)014<0676:NAIVOR>2.0.CO;2.
- , and J. Willebrand, 2001: Mechanism of interannual to decadal variability of the North Atlantic circulation. *J. Climate*, **14**, 2266–2280, doi:10.1175/1520-0442(2001)014<2266:MOITDV>2.0.CO;2.
- Farneti, R., and G. K. Vallis, 2011: Mechanisms of interdecadal climate variability and the role of ocean–atmosphere coupling. *Climate Dyn.*, **36**, 289–308, doi:10.1007/s00382-009-0674-9.
- Gent, P. R., and Coauthors, 2011: The Community Climate System Model version 4. *J. Climate*, **24**, 4973–4991, doi:10.1175/2011JCLI4083.1.
- Goosse, H., H. Renssen, F. M. Sellen, R. J. Haarsma, and J. D. Opsteegh, 2002: Potential causes of abrupt climate events: A numerical study with a three-dimensional climate model. *Geophys. Res. Lett.*, **29**, 1860, doi:10.1029/2002GL014993.
- Häkkinen, S., P. B. Rhines, and D. L. Worthen, 2011: Atmospheric blocking and Atlantic multidecadal ocean variability. *Science*, **334**, 655–659, doi:10.1126/science.1205683.
- Hall, A., and R. J. Stouffer, 2001: An abrupt climate event in a coupled ocean–atmosphere simulation without external forcing. *Nature*, **409**, 171–175, doi:10.1038/35051544.
- Huber, C., and Coauthors, 2006: Isotope calibrated Greenland temperature record over Marine Isotope Stage 3 and its relation to CH₄. *Earth Planet. Sci. Lett.*, **243**, 504–519, doi:10.1016/j.epsl.2006.01.002.
- Jackson, L., and M. Vellinga, 2013: Multidecadal to centennial variability of the AMOC: HadCM3 and a perturbed physics ensemble. *J. Climate*, **26**, 2390–2407, doi:10.1175/JCLI-D-11-00601.1.
- Jochum, M., A. Jahn, S. Peacock, D. A. Bailey, J. T. Fasullo, J. Kay, S. Levis, and B. Otto-Bliesner, 2012: True to Milankovitch: Glacial inception in the new Community Climate System Model. *J. Climate*, **25**, 2226–2239, doi:10.1175/JCLI-D-11-00044.1.
- Johns, W., T. Shay, J. Bane, and D. Watts, 1995: Gulf Stream structure, transport, and recirculation near 68°W. *J. Geophys. Res.*, **100**, 817–838, doi:10.1029/94JC02497.
- Kageyama, M., and Coauthors, 2013: Climatic impacts of fresh water hosing under Last Glacial Maximum conditions: A multi-model study. *Climate Past*, **9**, 935–953, doi:10.5194/cp-9-935-2013.
- Kalnay, E., and Coauthors, 1996: The NCEP/NCAR 40-Year Reanalysis Project. *Bull. Amer. Meteor. Soc.*, **77**, 437–471, doi:10.1175/1520-0477(1996)077<0437:TNYRP>2.0.CO;2.
- Kim, J.-H., O. E. Romero, G. Lohmann, B. Donner, T. Laepple, E. Haam, and J. S. S. Damste, 2012: Pronounced subsurface cooling of North Atlantic waters off northwest Africa during

- Dansgaard–Oeschger interstadials. *Earth Planet. Sci. Lett.*, **339**, 95–102, doi:10.1016/j.epsl.2012.05.018.
- Landais, A., and Coauthors, 2004: A continuous record of temperature evolution over a sequence of Dansgaard–Oeschger events during Marine Isotopic Stage 4 (76 to 62 kyr BP). *Geophys. Res. Lett.*, **31**, L22211, doi:10.1029/2004GL021193.
- Li, C., and D. S. Battisti, 2008: Reduced Atlantic storminess during Last Glacial Maximum: Evidence from a coupled climate model. *J. Climate*, **21**, 3561–3579, doi:10.1175/2007JCLI2166.1.
- , —, D. P. Schrag, and E. Tziperman, 2005: Abrupt climate shifts in Greenland due to displacements of the sea ice edge. *Geophys. Res. Lett.*, **32**, L19702, doi:10.1029/2005GL023492.
- , —, and C. M. Bitz, 2010: Can North Atlantic sea ice anomalies account for Dansgaard–Oeschger climate signals? *J. Climate*, **23**, 5457–5475, doi:10.1175/2010JCLI3409.1.
- Liu, Z., Z. Lu, X. Wen, B. Otto-Bliesner, A. Timmermann, and K. Cobb, 2014: Evolution and forcing mechanisms of El Niño over the past 21,000 years. *Nature*, **515**, 550–553, doi:10.1038/nature13963.
- Locarnini, R., A. Mishonov, J. Antonov, T. Boyer, H. Garcia, O. Baranova, M. Zweng, and D. Johnson, 2010: *Temperature*. Vol. 1, *World Ocean Atlas 2009*, NOAA Atlas NESDIS 68, 184 pp.
- Manabe, S., and R. J. Stouffer, 1999: Are two modes of thermohaline circulation stable? *Tellus*, **51A**, 400–411, doi:10.1034/j.1600-0870.1999.t01-3-00005.x.
- Martin, T., W. Park, and M. Latif, 2015: Southern Ocean forcing of the North Atlantic at multi-centennial time scales in the Kiel Climate Model. *Deep-Sea Res. II*, **113**, 39–48, doi:10.1016/j.dsr2.2014.01.018.
- Merkel, U., M. Prange, and M. Schulz, 2010: ENSO variability and teleconnections during glacial climates. *Quat. Sci. Rev.*, **29**, 86–100, doi:10.1016/j.quascirev.2009.11.006.
- Mignot, J., A. Ganopolski, and A. Levermann, 2007: Atlantic subsurface temperatures: Response to a shutdown of the overturning circulation and consequences for its recovery. *J. Climate*, **20**, 4884–4898, doi:10.1175/JCLI4280.1.
- Moy, C. M., G. O. Seltzer, D. T. Rodbell, and D. M. Anderson, 2002: Variability of El Niño/Southern Oscillation activity at millennial timescales during the Holocene epoch. *Nature*, **420**, 162–165, doi:10.1038/nature01194.
- O'Brien, S. R., P. A. Mayewski, L. D. Meeker, D. A. Meese, M. S. Twickler, and S. I. Whitlow, 1995: Complexity of Holocene climate as reconstructed from a Greenland ice core. *Science*, **270**, 1962–1964, doi:10.1126/science.270.5244.1962.
- Palmer, T. N., 1993: Extended-range atmospheric prediction and the Lorenz model. *Bull. Amer. Meteor. Soc.*, **74**, 49–65, doi:10.1175/1520-0477(1993)074<0049:ERAPAT>2.0.CO;2.
- Pausata, F., C. Li, J. Wettstein, M. Kageyama, and K. Nisancioglu, 2011: The key role of topography in altering North Atlantic atmospheric circulation during the last glacial period. *Climate Past*, **7**, 1089–1101, doi:10.5194/cp-7-1089-2011.
- Pedlosky, J., 1996: *Ocean Circulation Theory*. Springer, 453 pp.
- Peltier, W. R., and G. Vettoretti, 2014: Dansgaard–Oeschger oscillations predicted in a comprehensive model of glacial climate: A “kicked” salt oscillator in the Atlantic. *Geophys. Res. Lett.*, **41**, 7306–7313, doi:10.1002/2014GL061413.
- Pickart, R. S., D. J. Torres, and R. A. Clarke, 2002: Hydrography of the Labrador Sea during active convection. *J. Phys. Oceanogr.*, **32**, 428–457, doi:10.1175/1520-0485(2002)032<0428:HOTLSD>2.0.CO;2.
- Rahmstorf, S., 2002: Ocean circulation and climate during the past 120,000 years. *Nature*, **419**, 207–214, doi:10.1038/nature01090.
- Rasmussen, T. L., and E. Thomsen, 2004: The role of the North Atlantic drift in the millennial timescale glacial climate fluctuations. *Palaeogeogr. Palaeoclimatol. Palaeoecol.*, **210**, 101–116, doi:10.1016/j.palaeo.2004.04.005.
- Rohling, E., and Coauthors, 2008: New constraints on the timing of sea level fluctuations during early to middle marine isotope stage 3. *Paleoceanography*, **23**, PA3219, doi:10.1029/2008PA001617.
- Sardeshmukh, P. D., and B. J. Hoskins, 1988: The generation of global rotational flow by steady idealized tropical divergence. *J. Atmos. Sci.*, **45**, 1228–1251, doi:10.1175/1520-0469(1988)045<1228:TGOGRF>2.0.CO;2.
- , G. P. Compo, and C. Penland, 2000: Changes of probability associated with El Niño. *J. Climate*, **13**, 4268–4286, doi:10.1175/1520-0442(2000)013<4268:COPAWE>2.0.CO;2.
- Schmittner, A., J. Green, and S. Wilmes, 2015: Glacial ocean overturning intensified by tidal mixing in a global circulation model. *Geophys. Res. Lett.*, **42**, 4014–4022, doi:10.1002/2015GL063561.
- Seager, R., and D. S. Battisti, 2007: Challenges to our understanding of the general circulation: Abrupt climate change. *Global Circulation of the Atmosphere*, Princeton University Press, 331–371.
- Shields, C. A., D. A. Bailey, G. Danabasoglu, M. Jochum, J. T. Kiehl, S. Levis, and S. Park, 2012: The low-resolution CCSM4. *J. Climate*, **25**, 3993–4014, doi:10.1175/JCLI-D-11-00260.1.
- Siddall, M., E. J. Rohling, A. Almqvist-Labin, C. Hemleben, D. Meischner, I. Schmelzer, and D. Smeed, 2003: Sea-level fluctuations during the last glacial cycle. *Nature*, **423**, 853–858, doi:10.1038/nature01690.
- Sidorenko, D., and Coauthors, 2015: Towards multi-resolution global climate modeling with ECHAM6-FESOM. Part I: Model formulation and mean climate. *Climate Dyn.*, **44**, 757–780, doi:10.1007/s00382-014-2290-6.
- Steffensen, J. P., and Coauthors, 2008: High-resolution Greenland ice core data show abrupt climate change happens in few years. *Science*, **321**, 680–684, doi:10.1126/science.1157707.
- Stocker, T. F., and S. J. Johnsen, 2003: A minimum thermodynamic model for the bipolar seesaw. *Paleoceanography*, **18**, 1087, doi:10.1029/2003PA000920.
- Stott, L., C. Poulsen, S. Lund, and R. Thunell, 2002: Super ENSO and global climate oscillations at millennial time scales. *Science*, **297**, 222–226, doi:10.1126/science.1071627.
- Timmermann, A., S. J. Lorenz, S.-I. An, A. Clement, and S.-P. Xie, 2007: The effect of orbital forcing on the mean climate and variability of the tropical Pacific. *J. Climate*, **20**, 4147–4159, doi:10.1175/JCLI4240.1.
- Ting, M., and P. D. Sardeshmukh, 1993: Factors determining the extratropical response to equatorial diabatic heating anomalies. *J. Atmos. Sci.*, **50**, 907–918, doi:10.1175/1520-0469(1993)050<0907:FDTERT>2.0.CO;2.
- Trenberth, K. E., G. W. Branstator, D. Karoly, A. Kumar, N.-C. Lau, and C. Ropelewski, 1998: Progress during TOGA in understanding and modeling global teleconnections associated with tropical sea surface temperatures. *J. Geophys. Res.*, **103**, 14 291–14 324, doi:10.1029/97JC01444.
- Tudhope, A. W., and Coauthors, 2001: Variability in the El Niño–Southern Oscillation through a glacial–interglacial cycle. *Science*, **291**, 1511–1517, doi:10.1126/science.1057969.
- Wunsch, C., 2006: Abrupt climate change: An alternative view. *Quat. Res.*, **65**, 191–203, doi:10.1016/j.yqres.2005.10.006.
- Yeager, S., and G. Danabasoglu, 2014: The origins of late-twentieth-century variations in the large-scale North Atlantic circulation. *J. Climate*, **27**, 3222–3247, doi:10.1175/JCLI-D-13-00125.1.
- Zhang, X., G. Lohmann, G. Knorr, and C. Purcell, 2014: Abrupt glacial climate shifts controlled by ice sheet changes. *Nature*, **512**, 290–294, doi:10.1038/nature13592.